A disease modelling approach for Angelman syndrome based on neuronal differentiation of patient-derived iPSCs

Ana Isabel da Silva Guerreiro

Thesis to Obtain the Master of Science Degree in

Biological Engineering

Supervisors: Professor Tiago Paulo Gonçalves Fernandes
Doctor Simão Teixeira da Rocha

Examination Committee

Chairperson: Professor Gabriel António Amaro Monteiro
Supervisor: Doctor Simão Teixeira da Rocha
Member of the Committee: Doctor Evguenia Pavlovna Bekman

October 2018

Acknowledgments

All the work that was developed by me for this dissertation was only possible to be accomplished with the support, perseverance and dedication of several people, to whom I am really grateful and I wish to acknowledge.

First of all, I want to thank Professor Joaquim Sampaio Cabral for receiving me in the SCBL team and for having given me the possibility of working in SCBL. I also want to thank Professor Maria do Carmo Fonseca for the partnership, allowing me to have the opportunity to work at iMM in Carmo-Fonseca Lab.

I would also like to thank my supervisors, Doctor Tiago Fernandes and Doctor Simão Rocha. Doctor Tiago Fernandes, I am sincerely grateful for all the help, sympathy and dedication demonstrated since my first days in Tagus. Thank you for your support, sharing of knowledge and valuable contributions to my work. I am very indebted for all the guidance, help in the lab, patience and availability in discussing results and for all the new ideas that enriched my work. Doctor Simão Rocha, I am grateful for the exemplary guidance with a rigorous scientific level, vigorous commitment, which contributed to enrich, step by step, all the stages underlying the work performed. Thank you for all the support in the lab tasks every time I asked you for assistance and for being always available to discuss results, giving new ideas and advising me. It was a great pleasure and honor to be supervised by both of you!

Ana Rita, my “unofficial” supervisor, all the words are few to thank you for everything you have done for me from the first moments, introducing me, teaching me all the different techniques in the lab, planning and discussing my work every time I questioned you. Thank you also for being always there with your contagious happiness and joy, even during weekends or in the endless hours in confocal microscopy, even having lots of other things to do. All your patience, perseverance and support were incredible. Thank you once again for the time you devoted to review and make suggestions regarding the manuscript and other important things during my time in SCBL.

Thank you also to Doctor Cláudia Miranda, Doctor Teresa Silva, and Mariana Branco for all your assistance in my integration in the lab, always available to help and clarify all my doubts with such a good mood, kindness and sympathy.

I also want to thank to Sara Morini and Diogo Nogueira, the “Team Cake” and the energy and vivacity of the SCBL. Sara Morini, thank you for the good humour in the lab and for all the advices, shared knowledge and for cheering me up with your contagious happiness when things did not go so well. Diogo Nogueira, thank you for all your help and support in numerous tasks in the lab, all the teachings about flow cytometry, for our discussions, your friendship and for your inexhaustible help during these months.

I want to thank my master team colleagues, Ana Sofia Borges, Silvia Gonella, Laura Sordini, Rodrigo Pedroso, Filipe Godinho, Cristiana Ulpiano, Tiago Ligeiro and the more recently master student Joana Saraiva for having received me so well, for all the support, care and mutual aid during these months. Thank you also for the help with the lab tasks, for all the brainstorms that allowed my work to be better and for an excellent work environment, even at weekends.

Regarding iMM group, I want to thank Ana Raposo, for teaching and helping me patiently the RNA/DNA extraction and RT-qPCR techniques and for being a valuable help always available to support and supervise my work in iMM. Also, I want to thank to Inês Godinho for the precious help in some experiments in addition to Maria Arez, for assisting me with COBRA assays.

I also want to thank all the other people in SCBL and iMM who I have not mentioned before, for being amazing colleagues and for welcoming me upon my arrival with such will to assist and support me, which created a great work environment.

Thank you to all my friends but specially Inês Henriques, Inês Sousa and Andreia Jardim. My gratitude is enormous to you! Inês Henriques, thank you for all the support, perseverance laughter, jokes and happiness that you brought to my life in this 14 years of friendship that will last for the rest of my entire life. Inês Sousa and Andreia Jardim, thank you all the assistance, patience and support during these months of pressure and anxiety. Thank you for all the good moments we spent together and the hard battles we waged side by side. Your friendship is something that I want to certainly keep for as long as possible!

Special thanks to Carlos Faria, for all the support, patience and for believing in me and in my value, even when I did not believe in myself. Thank you for being such a good listener who was always present in both good but mainly in the not so good moments, always having a word of comfort to encourage me in those stressing moments.

I also want to thank to all the teachers and professors that have passed through my life and stimulated my interest in knowing more and more. I would especially like to thank all those who have motivated my growing taste for science and for making me discover the wonderful and challenging world of stem cells.

Finally, I have to thank to my family, especially to my sister and my parents. My beloved Sister, thank you for everything you have done for me, for all the precious advices, for all the teachings you gave me. Thank you for understanding every time I could not be present because of the thesis and for all the patience and support during these months. My dear parents, thank you for all the advice, teachings and values that allowed me to be the person I am today. Thank you for all the sacrifices you have made throughout your life so that I could have a good education and be where I am today.
Without you it would not have been possible!

Abstract

Angelman syndrome (AS) is a neurodevelopmental disorder caused by deficiency of maternally inherited *UBE3A* gene, which displays paternal imprinting. Regarding the promising features of human induced pluripotent stem cells (hiPSCs), a robust disease modelling system was created, mimicking the neurogenesis process *in vitro*. For that, control and patient-derived iPSCs were differentiated using the dual-SMAD inhibition protocol. Characterization of the iPSCs population confirmed a pluripotent state of these cells before the neural commitment protocol. Neural commitment of both control and AS patient derived iPSCs was monitored by immunofluorescence (IF) and RT-qPCR for several differentiation markers from day 12 to day 80. Successful neural induction was achieved for both control and AS-derived iPSCs. During this neuronal protocol, the methylation status of the PWS-IC which controls imprinting regulation of the Angelman locus was shown to be correctly maintained, which assures the feasibility of this protocol to model AS. Finally, *UBE3A* expression was also monitored and shown to increase during differentiation of the control iPSC-derived neurons and to be always higher than in AS iPSC-derived neurons, where a gradual decay of *UBE3A* expression is noticed. However, at the last timepoint studied (day 80), *UBE3A* expression is not entirely switch off in AS iPSC-derived neurons, suggesting that a longer differentiation period might be necessary for the paternal *UBE3A* to be completely silenced. Taken together, the results suggest that dual-SMAD inhibition protocol for neuronal differentiation provide a good system to model AS syndrome which is able to discern phenotypes between control and AS iPSC-derived neurons.

Keywords: Angelman Syndrome, *UBE3A*, Genomic imprinting, Human induced pluripotent stem cells (hiPSCs), Neuronal differentiation

Resumo

O síndrome de Angelman (AS) é um distúrbio do neuro-desenvolvimento causado pela deficiência do gene UBE3A herdado pela mãe, exibindo *imprinting* paternal. Tendo em conta as características promissoras das células estaminais pluripotentes induzidas humanas (hiPSCs), foi criado um sistema robusto de modelação de doenças, mimetizando o processo de neurogénese *in vitro*. As iPSCs do controlo e paciente foram diferenciadas usando o protocolo *dual-SMAD inhibition*. A caracterização da população de iPSCs confirmou um estado pluripotente dessas células antes do protocolo de comprometimento neural. Durante esse protocolo as iPSCs foram monitorizadas por imunofluorescência (IF) e RT-qPCR para vários marcadores de diferenciação do dia 12 ao 80. A indução neural foi bem sucedida tanto para iPSCs controlo e do paciente. Durante este protocolo, o estado de metilação do PWS-IC que controla a regulação do *imprinting* do *locus* Angelman mostrou-se corretamente mantido, o que garante a viabilidade deste protocolo para modelar o AS. Finalmente, a expressão de *UBE3A* aumentou durante a diferenciação dos neurónios do controlo, sendo sempre superior à dos derivados do paciente, onde um decaimento gradual da expressão de *UBE3A* é notado. No entanto, no dia 80 a expressão de *UBE3A* não é totalmente cessada em neurónios derivados do paciente, sugerindo que um período de diferenciação mais longo pode ser necessário para que o *UBE3A* paterno seja completamente silenciado. Em conjunto, os resultados sugerem que o protocolo de *dual-SMAD inhibition* para diferenciação neuronal fornece um bom sistema para modelar o AS, sendo capaz de discernir fenótipos entre neurónios do controlo e paciente.

Palavras-chave: Síndrome de Angelman, *UBE3A*, *Imprinting* genómico, Células estaminais pluripotentes induzidas humanas (hiPSCs), Diferenciação neuronal

List of Contents

List of tables

List of figures

List of abbreviations

AAV – Adeno-associated virus
AP – Action potential
AS – Angelman Syndrome
ASD – Autism Spectrum Disorder
AS-IC – Angelman Syndrome Imprinting center
ASO – Antisense oligonucleotide
bFGF – Basic fibroblast growth factor
cDNA – Complementary deoxyribonucleic acid
COBRA – Combined bisulfite restriction analysis
CNS –Central Nervous System
DAPI – 4',6-diamidino-2-phenylindole
DMSO – Dimethyl sulfoxide
DMEM - Dulbecco's Modified Eagle Medium
DNA - Deoxyribonucleic acid
EDTA – Ethylenediaminetetraacetic acid
ECCs – Embryonal carcinoma cells
EGCs – Embryonic germ cells
ESCs – Embryonic stem cell
FDA – Food and Drug Administration
GAD – Glutamic acid decarboxylase
GAPDH – Glyceraldehyde 3-phosphate dehydrogenase
GFAP – Glial fibrillary acidic protein
hESCs – Human embryonic stem cells
hiPSCs – Human induced Pluripotent Stem Cells
hPSCs – Human pluripotent stem cells
IC – Imprinting center
ICM – Inner cell mass
IF – Immunofluorescence
KO-SR – KnockOut^{TM} -DMEM/SerumReplacement
lncRNA – Long noncoding RNA
Map2 – Microtubule-associated protein 2
MECP2 – Methyl-CpG-binding protein 2
NEPs – Neuroepithelial progenitors
NeuN – Neuronal Nuclei
NPCs – Neural progenitor cells
Oct4 – Octamer-binding transcription factor 4
OLs – Oligodendrocytes
Pax6 – Paired box 6

PBS – Phosphate-buffered saline

PFA – Paraformaldehyde

P/S – Penicillin/streptavidin

PSC – Pluripotent stem cells

PWS – Prader-Willi Syndrome

PWS-IC – Prader-Willi Syndrome imprinting center

RMP – Resting membrane potential

RT-qPCR – Quantitative real-time PCR

snoRNA – Small nucleolar RNA

SSEA – Stage-specific embryonic antigen

S100 β – S-100 Protein Subunit Beta

TUJ1 – β-III-tubulin

***UBE3A*-ATS** – *UBE3A* Antisense

UPD – Uniparental disomy

I. Introduction

I.1. Angelman Syndrome

Angelman syndrome (AS) is a severe neurodevelopmental disorder characterized by intellectual disability, developmental delay, speech impairment, seizures and ataxia that does not enable the patients to live in an independent manner [1,2]. AS is a rare disease, being present in one in 12,000 - 20,000 of the population[1,2,3] .

AS is caused by loss of function of the maternally inherited copy of the *UBE3A* imprinted genes and can be triggered by four distinct molecular mechanisms: large maternal deletions of chromosome 15q11-q13 (accounts for 70–80 %); mutations in the maternally inherited copy of *UBE3A* gene (10–20 %); imprinting defects causing modifications in the expression of maternally inherited *UBE3A* copy (3–5 %) and uniparental disomy (UPD) , which occurs when the two homologues of a chromosome pair are originated from the same parent with no homologue from the other parent [4,5,6]. Phenotype severity is connected with the type of mutation, with the full deletion of chromosome 15q11-13 the most severe, while point mutations in *UBE3A,* the less severe [7] .

I.1.1. Symptoms

Individuals with AS have global developmental delay that evolves to severe intellectual disability, with their language skills being more delayed than their motor skills, and their expressive language being far more delayed than their receptive language, usually having only minimal speech [8]. Although the majority of skills are delayed, there is some variability in adaptive behavior functioning, with relative strength in socialization and relative weakness in motor skills [9].

AS patients present phenotypes and behaviors which differ, taking into account the various age groups throughout life. Newborns typically display a normal phenotype and developmental delays are primarily noticed around 6 months of age [3]. By the first year of age, development delays in AS are usually evident with delayed attainment of gross motor, fine motor, receptive language, expressive language, and social skills. Reportedly, an individual with AS plateau at a developmental level of between 24 and 30 months, and cognitive performance is usually in the range of severe functional impairment [10].

In addition, most individuals with this disease go through long periods in which they may exhibit sleep disturbances evidenced by difficulties in falling asleep and multiple awakenings at night. Other neurological features include ataxia, epilepsy, and tremors mostly exhibited in older children or adults and generalized hypotonia, characterized by a varied spectrum of low tone muscle anomalies in

younger individuals that could progress to peripheral hypertonia (high tone muscle anomalies) in older individuals [8,11].

I.1.2. *UBE3A* gene and the chromosome 15q11-q13 imprinted locus

UBE3A belongs to a small subgroup of genes known as imprinted genes. These genes are expressed monoallelically depending on parent of origin of the alleles. In the case of *UBE3A*, its imprinting status is tissue-specific .Whereas in most tissues, *UBE3A* is biallelically expressed, in the brain and particularly in neurons, the paternally derived *UBE3A* gene is silenced, and only the maternally inherited copy remains active [10]. *UBE3A* encodes an ubiquitin-protein ligase E3A, which is also known as E6AP ubiquitin-protein ligase or human papillomavirus E6-associated protein [2]. UBE3A protein might function as an E3 component of the ubiquitin cycle targeting protein substrates to the proteasome for degradation, however direct targets remain hardly identified [12].
UBE3A protein localizes to the nuclei and to a lesser extent the dendrites of neurons as well as to their pre- and postsynaptic compartments [13]. Mice that lacked maternal expression of *UBE3A* have reduced dendritic spine length and density, suggesting a role in synaptic formation at the structural level [13].

Genomic imprinting in 15q11-q13 locus is controlled by a bipartite imprinting center (IC) constituted by two elements: the Prader-Willi syndrome imprinting center (PWS-IC) and the Angelman syndrome imprinting center (AS-IC) separated by 35 kb [10,14] (figure I. 1). PWS-IC includes the major promoter and exon 1 of the *SNURF-SNRPN* gene. Within the PWS-IC lies a differentially-methylated region that is methylated on the maternally-inherited allele and unmethylated on the paternally-inherited allele. AS-IC that is thought to establish the maternal imprint of the PWS-IC in the maternal germline by driving expression from the upstream exons of the *SNURF-SNRPN* bicistronic gene [14].

The *SNURF-SNRPN* gene encodes a bicistronic transcript that produces two proteins: SNURF and SNRPN [15]. SNRPN is a small nuclear ribonucleoprotein that functions in pre-mRNA processing and likely in alternative splicing. SNURF is a nuclear localized protein of unknown function that is produced from the first three exons of the *SNURF-SNRPN* transcript [14]. The *SNRPN* locus also produces several non-coding RNAs including small nucleolar RNAs (snoRNAs) and long non-coding RNAs (lncRNAs) and undertakes extensive alternative splicing, a phenomenon not fully described or understood [14].

In the majority of somatic cells, the *SNRPN* transcript is terminated at or upstream of a non-coding transcript with unknown function called *IPW*, and includes the *SNORD116* snoRNA cluster [16]. In neurons the transcription continues further to regions which include the *SNORD115* snoRNAs and the *UBE3A* antisense transcript (*UBE3A-ATS*), a long non-coding RNA transcribed in the antisense orientation and overlaps the UBE3A gene[14]. It is believed that paternal silencing of the *UBE3A* copy is regulated by this *UBE3A-ATS* transcript as *UBE3A* itself is not differentially methylated [10,17,18].

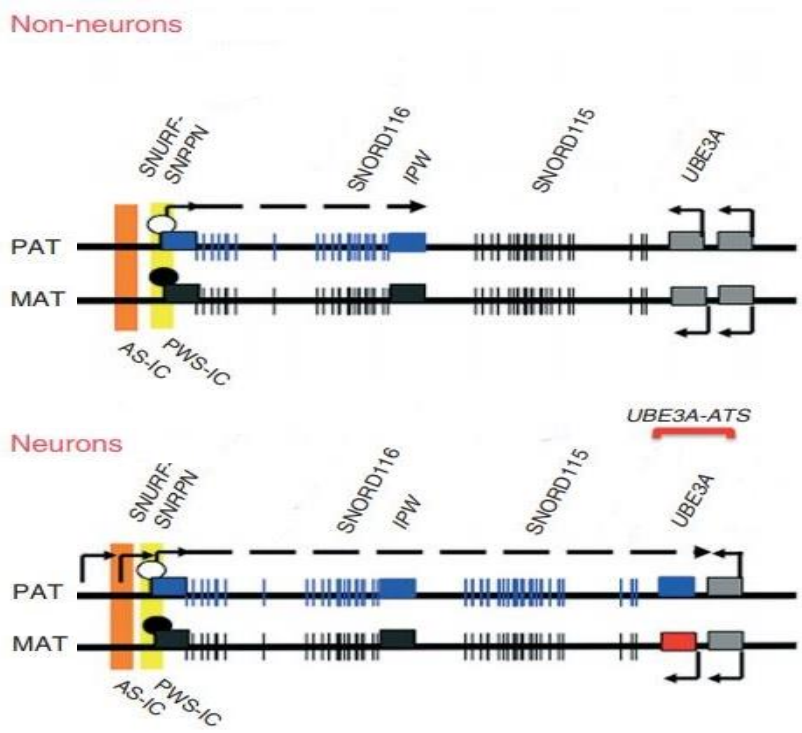

Figure I. 1 : Map of the human chromosome 15q11-q13 imprinted region indicating methylation status and gene expression patterns in non-neurons (top) and neurons (bottom). Blue rectangles represent imprinted transcripts that are paternally expressed, red rectangles represent imprinted transcripts that are maternally expressed, black rectangles represent the repressed alleles of imprinted genes, and grey rectangles represent biallelically expressed transcripts. AS-IC corresponds to the Angelman Syndrome imprinting center and PWS-IC represents the Prader-Willi Syndrome imprinting center; the white circles represent unmethylated PWS-IC whereas the black circles represent methylated PWS-IC. (Adapted from [14])

I.1.3. Diagnosis and Treatment

It can take several years before the correct clinical diagnosis of AS is made. The diagnosis is usually first suspected on the basis of the behavioral phenotype, particularly combinations of movement disorder, absent speech, and happy demeanor [3].

When a case of AS is suspected, the first test for AS is a DNA methylation evaluation of the PWS-IC at the chromosome 15q11-13 region. The test uses either methylation-specific polymerase chain reaction or methylation-sensitive multiplex ligation-dependent probe amplification. If the DNA methylation test is positive, supplementary testing is needed to distinguish between large maternal deletions, paternal UPD or imprinting defects (figure I. 2) [10,19]. If DNA methylation analysis is negative, then sequencing of the *UBE3A* gene is suitable for those with a conclusive AS phenotype. When both *UBE3A* mutation and DNA methylation analysis and testing are negative, the possibility of AS is small, and it might be another disease displaying a similar phenotype [10]. Reappearance risk for AS due to large deletion or UPD is minor.

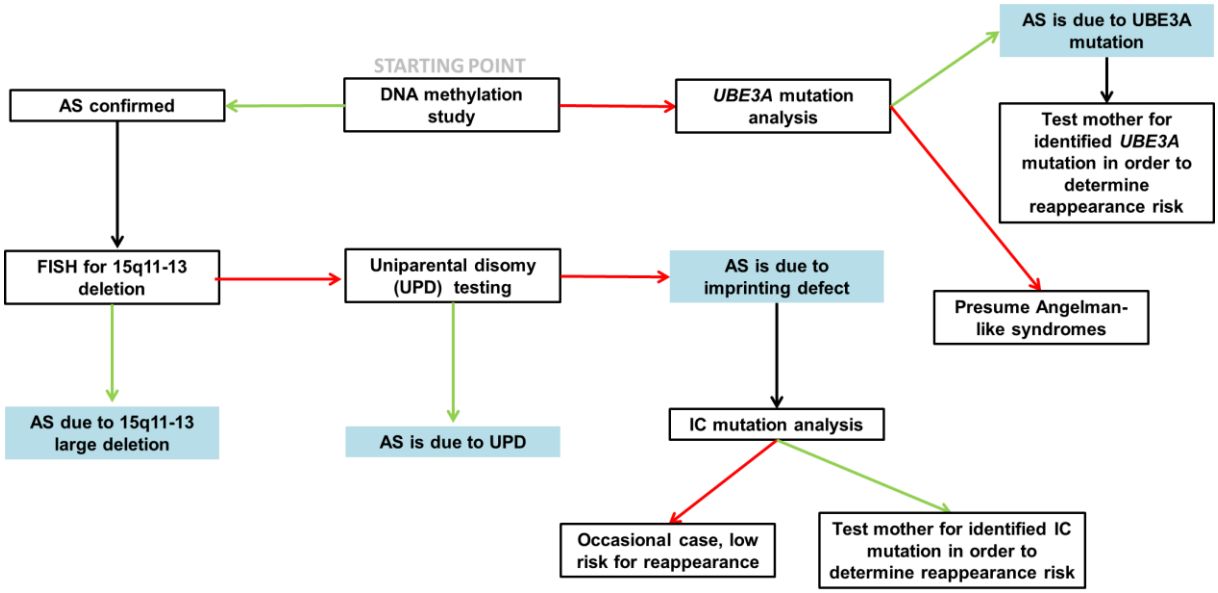

Figure I. 2: Molecular diagnostic algorithm for Angelman Syndrome. Green arrows represent positive tests and red arrows negative tests AS: Angelman Syndrome, FISH: Fluorescent in situ hybridization, IC: Imprinting center, UPD: Uniparental disomy (Adapted from [10])

Despite a clear understanding of the disease-causing events in AS, there are currently no AS-specific systematic treatments for patients [1,20]. Further investigation of the roles played by UBE3A protein in the central nervous system (CNS) and the way its imprinting is regulated is required for developing effective therapies [21].

I.1.3.1 Therapeutic methodologies under development

In neurons, the paternal allele of *UBE3A* is intact but epigenetically silenced, raising the prospect that AS could be treated by activating this silenced allele to restore functional *UBE3A* protein [22] .Regarding this possibility, several groups have attempted to restore *UBE3A* expression by direct gene therapy or by un-silencing the paternal allele [21].

In 2011, Daily and his collaborators performed the injection of recombinant adeno-associated virus (AAV) carrying the mouse *UBE3A* into the hippocampus of AS mice which resulted in local restoration of *UBE3A* expression and improvement of hippocampus-dependent learning and memory [23]. Nevertheless, the viral vectors exhibited limited distribution beyond the hippocampus and there was no effect on motor dysfunction. Moreover, this approach revealed additional concerns regarding the precise control of *UBE3A* expression, since high *UBE3A* levels are a risk factor for autism spectrum disorder (ASD) [21].

In 2012, Huang and his collaborators identified several topoisomerase inhibitors that caused the unsilencing of the paternal *UBE3A* allele, namely twelve topoisomerase I and four topoisomerase II inhibitors. For this purpose they used an unbiased approach in primary cortical neurons from *UBE3A*-Yellow Fluorescent Protein knock-in mice [22]. Through these studies it has been demonstrated that a

topoisomerase I inhibitor named topotecan caused the inhibition of *UB3A-ATS* transcription leading to the reactivation of the paternal copy of *UBE3A* in AS mouse [21,22]. When administered in vivo, topotecan was able to reactivate the paternal allele of *UBE3A* in several regions of the central nervous system and this expression was maintained for at least 12 weeks after treatment with this inhibitor. This results suggested that this topoisomerase inhibition can have durable effects on gene expression [22].

Posterior studies performed in 2013 by Powell and his co-workers prove that topotecan treatment stabilizes the formation of RNA-DNA hybrids at repeat elements within paternal *Snord116*, corresponding to increased chromatin decondensation and inhibition of *Ube3a-ats* expression. Neural progenitor cells (NPCs) from paternal Snord116 deletion mice display increased *Ube3a-ats l*evels in differentiated neurons and show a reduced effect of topotecan compared with wild-type neurons [24]. Since topotecan is a Food and Drug Administration (FDA) approved anti-cancer drug, the results gave hope for rapidly developing the drug as a potential therapy for AS. However, topotecan lack of specificity and toxicity have obstructed further advancement of the drug as an AS treatment [21].

In 2015, a study conducted by Meng and his co-workers used antisense oligonucleotides (ASOs) against Ube3a-ats in AS mice [21]. ASOs are short, synthetic, single-stranded oligodeoxynucleotides that can modify RNA and reduce, restore, or alter protein expression through several distinct mechanisms. By targeting the source of the pathogenesis, ASO-mediated therapies have an higher chance of success than therapies targeting downstream pathways [25]. ASO treatment was commonly well tolerated showing a specific reduction of Ube3a-ats and the unsilencing of paternal Ube3a in neurons *in vitro* and *in vivo* [1,21]. Partial restoration of Ube3a protein in an AS mouse model ameliorated some cognitive deficits associated with the disease [1]. After a single ASO dose, Ube3a-ats reduction was sustained for 16 weeks in the CNS, and returned to basal expression by 20 weeks after treatment [21]. Indeed, some features of this ASO drugs, namely the long-term action, broad tissue distribution and well-tolerated delivery can be proof that ASOs might be a viable therapeutic strategy for CNS diseases, particularly to activate expression of the paternal *UBE3A* allele in AS patients [1].
The use of modified ASOs against *UBE3A-ATS* is a promising therapeutic approach for AS. However, whether *UBE3A-ATS* downregulation is achievable using this approach in humans needs to be tested in tractable and appropriated human cellular system.

I.2. Stem Cells as platforms to study human diseases

I.2.1. Stem Cells

Stem cells are the foundation for every organ and tissue in our body. Stem cells are a specific group of cells with the ability to perpetuate themselves through self-renewal and under certain conditions give rise to several different types of cells that create an entire organism. Therefore, stem cells have the potential to develop into mature cells derived from the three germ layers (endoderm, ectoderm and mesoderm) through differentiation, that have characteristic shapes and specialized functions, such as heart cells, skin cells, or nerve cells [26,27,28].

According to the ability to self-renew and their potential degree of differentiation stem cells are mainly classified in four types: totipotent, pluripotent, multipotent stem cells and unipotent progenitors [27].

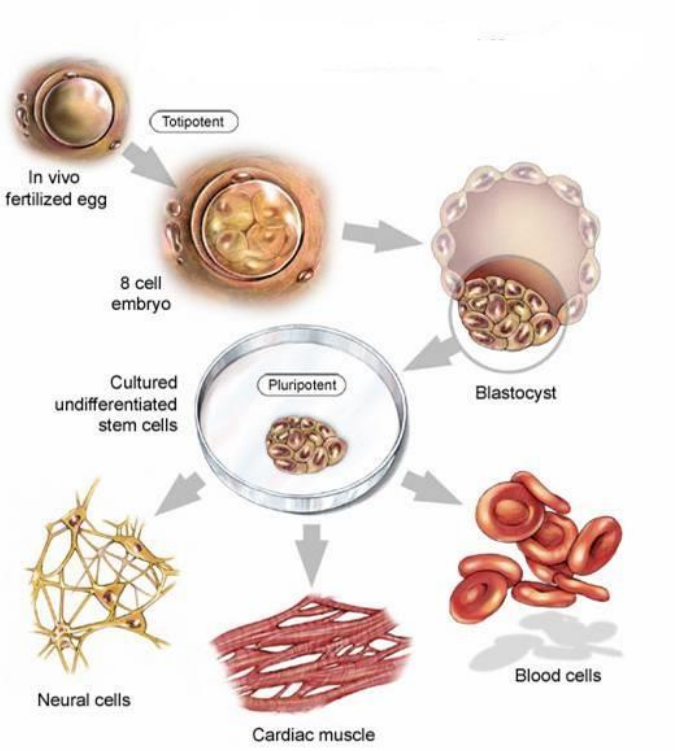

Figure I. 3 : Development of the different types of stem cells and its final cell fate (Adapted from [29])

The representation present in figure I.3 illustrates the decreasing potential of stem cells to generate multiple types of cells as they undergo differentiation.

Totipotent cells like the fertilized egg or zygote are the most developmentally expansive cells, which may not only give rise to all the cells and tissues comprising an embryo but also to extra-embryonic and placental tissue[30,31]. Indeed, totipotent stem cells can give rise to the whole organism[32]. On the other, pluripotent stem cells, such as embryonic stem cells (ESCs) are stem cells from the inner cell mass (ICM) which can give rise to differentiated cells from the three germ layers, but without generating extra-embryonic lineages [31,33] . ESCs can be isolated from the ICM of mammalian

blastocysts and have the ability to grow indefinitely *in vitro* and can thus be cultured as immortalized cell lines [31,33]. Multipotent or adult/somatic stem cells, depending on the type of classification, are lineage-committed cells found among specialized (differentiated) cells in a tissue or organ [27]. Tissue-constrained somatic stem cells are limited in their potency to the cell types of the tissue in which they reside. Despite earlier claims of greater plasticity, they do not differentiate into foreign cell types or tissues without considerable genetic or chemical manipulation [31]. Finally, unipotent stem cells are the more restricted ones, with the capability of differentiating into only one cell type [34]. Spermatogonial stem cells are unipotent as they can only give rise to Sperm [35,36].

I.2.2. Human pluripotent stem cells (hPSCs)

As previously mentioned, a single PSC is capable of differentiating into cells arising from the three germ layers that give rise to somatic cells of the body. PSCs were initially isolated from mouse embryos, but were then isolated from human embryos. Both human and mouse PSCs have unlimited self-renewal capacity, associated with high telomerase activity and undergo symmetric divisions in culture without differentiating [26,37]. In addition, human pluripotent stem cells represent a distinctive source for cell-based therapies and regenerative medicine. The intrinsic features of these cells such their capacity to be expanded indefinitely overcome some drawbacks of conventional adult stem cells [38]. There are numerous types of PSCs, ESCs, induced pluripotent stem cells (iPSCs), embryonic germ cells (EGCs) and embryonal carcinoma cells (ECCs) [26,27].

I.2.2.1. Human induced pluripotent stem cells (hiPSCs)

Until recently, human PSC could only be isolated from the ICM of the blastocyst, being designated ESCs [39,40]. Nevertheless, in 2007, Shinya Yamanaka and collaborators were capable to reprogram human somatic cells into the pluripotent stem cell state using ectopic expression of four transcription factors (*OCT4, SOX2, KLF4, c-MYC*) [33]. This seminal work was contemplated with the Nobel Prize award in Physiology or Medicine in 2012 (jointly with John Gurdon for their nuclear transfer work in 1960). Their findings were pivotal to show how mature somatic cells can be reprogrammed to acquire a pluripotency state, becoming pluripotent stem cells [33,41,42,43]. iPSCs are characterized by the ability to self-renew indeterminately, stable karyotype and the potential to differentiate into cell types of the three germ layers, e.g. ectoderm, mesoderm and endoderm [43]. These cells are also capable to form teratomas, such as ESCs, thus, they cannot be transplanted in the undifferentiated state to a human host. However, they can be produced from the somatic cells of any human patient, thus avoiding the problem of rejection, and the ethical issues associated with ESCs [33, 42,43,44] .

Regarding their unique features, iPSCs brought massive prospects into the biomedical field due to their potential applications in disease modelling, drug and toxicity screening, patient-tailored therapies

and engineered tissues, making possible the investigation of disease mechanisms, as well as to test for potential therapeutics [39,43,45,46].

I.3. Modelling neurogenesis *in vitro*

Many neurodegenerative diseases are progressive, complex diseases without clear mechanisms or effective treatments[47]. To better understand the pathogenesis of neurodegenerative disorders and to discover new drugs that prevent cell loss, a reliable in vitro modelling system that mimics the features of a particular disease is extremely necessary [47,48]. Recent advancement in stem cell research has opened new prospects to generate large numbers of several neural cell types in vitro and to use them for repair of the nervous system [49].

A few years ago, an approach based on the generation of post-mortem human neural primary cultures has been used for transplantation, with some promising results in some neurodegenerative diseases like Parkinson's disease and Huntington's disease [50,51]. However, this methodology is limited due to the availability of cells that can be obtained and the short lifetime of these primary cultures [52,53]. Despite the limitations presented in these studies, they were very useful since they provided evidence that functional restoration by neuronal replacement can work in the diseased human brain.

Nevertheless, some improved alternatives were created in order to perform neuronal differentiation *in vitro*, in a suitable way. An example of this approach is the derivation of autologous pluripotent stem cells, that is an alternative strategy to avoid graft rejection and immunosuppression [48].

I.3.1. Neural stem and progenitor cells

Neurogenesis in mammals begins with the induction into neuroectoderm, which causes the formation of a structure called neural plate. Then, this structure gives rise to the neural tube. The recently formed arrangements are made up by a layer of so-called neuroepithelial progenitors (NEPs), which are probably a complex and heterogeneous population, slightly more committed than neural progenitor cells (NPCs), that are self-renewing multipotent populations present in the developing and adult mammalian CNS, but with a more limited ability to self-renew [54,55,56].

During development, neural stem cells give rise to all the neurons of the mammalian CNS [57]. They generate the neurons and glia of the developing brain in response to appropriate developmental cues and also account for the limited regenerative potential of the adult brain [58]. *In vivo*, NPCs exist to support self-renewal, a process that is extended by the life-long persistence of NPCs within the restricted CNS area, and also the ability of this multipotent stem cells to clonally originate the CNS lineages – neurons (GABAergic and glutamatergic) and glial cells (astrocytes and oligodendrocytes)[54,58].

The GABAergic and glutamatergic neurons of the forebrain arise from different pools of progenitors. GABAergic neurons are generated essentially in the basal telencephalon, prethalamus, and

pretectum, whereas glutamatergic neurons arise from the dorsal telencephalon and dorsal thalamus [59].

GABAergic neurons, more specifically interneurons, synthesize GABA, the primary inhibitory neurotransmitter, from glutamate by glutamic acid decarboxylases (GADs). GADs exists in two isoforms, GAD65 and GAD67, each performing different roles within the neuron. GABAergic interneurons are highly heterogeneous in terms of multiple morphological, electrophysiological, and molecular properties [60,61].

Glutamatergic neurons express two major isoforms of Vesicular glutamate transporter (VGLUT). These two isoforms of VGLUT, namely VGLUT1 and VGLUT2 are present in the adult brain [62,63]. They are selectively expressed in functionally distinct subpopulations of glutamatergic neurons, and exhibit pathway-specific and target-specific expression in the glutamatergic neural circuits in the CNS [63,64].

Glial cells are the most abundant cell type in the CNS with a notable role in structure maintenance and functioning. These type of cells are derived from two main sources: radial glial cells (RGCs) within the ventricular zone and intermediate progenitors in the subventricular zone and are involved in almost every aspect of neural activity, playing critical roles in CNS functions, development, injury, and diseases [65,66,67,68].

Glial cells were traditionally divided into three categories: astrocytes, oligodendrocytes (OLs), and microglia. Astrocytes are the most abundant type of glial cells, comprising a heterogeneous group of cell subtypes that have a crucial role in brain function and development. Astrocytes consist of at least four distinct subtypes of glial fibrillary acidic protein (GFAP)-positive cells in the human brain, with two subtypes in rodents, demonstrating specie-specific differences among mammals [65].

I.3.2. Neuronal differentiation of hiPSCs

Since the derivation of iPSCs one decade ago, the understanding of the cues required to differentiate pluripotent cells into specific NPCs and functional neural subtypes has grown tremendously[69].

For neurodevelopmental disease modelling, the differentiation of iPSCs into candidate neural lineages is the key factor to recapitulating disease phenotypes. The differentiation protocol from iPSCs to neural progenitors is reminiscent on human embryonic development [47]. Beginning in a pluripotent state, these cells differentiate first into NPCs cells followed by the formation of neural rosettes, a neural tube-like structure in normal neurodevelopment [70] (Figure I. 4) . Neural rosettes contain NPCs resembling neuroepithelial and radial glial cells of the developing cortex that are radially organized to create a lumen, resembling the structure of the ventricular zone of the developing cortex [71,58]. These structures normally express early neuroectodermal markers, such as PAX6 and SOX1, and display also a positive immunostaining for SOX2, NESTIN and for the tight junction protein ZO-1 [58] . The rosette structures not only express proteins from neuroepithelial cells in the neural tube, but also can differentiate into several region-specific neuronal and glial cell types in response to proper stimuli [58].

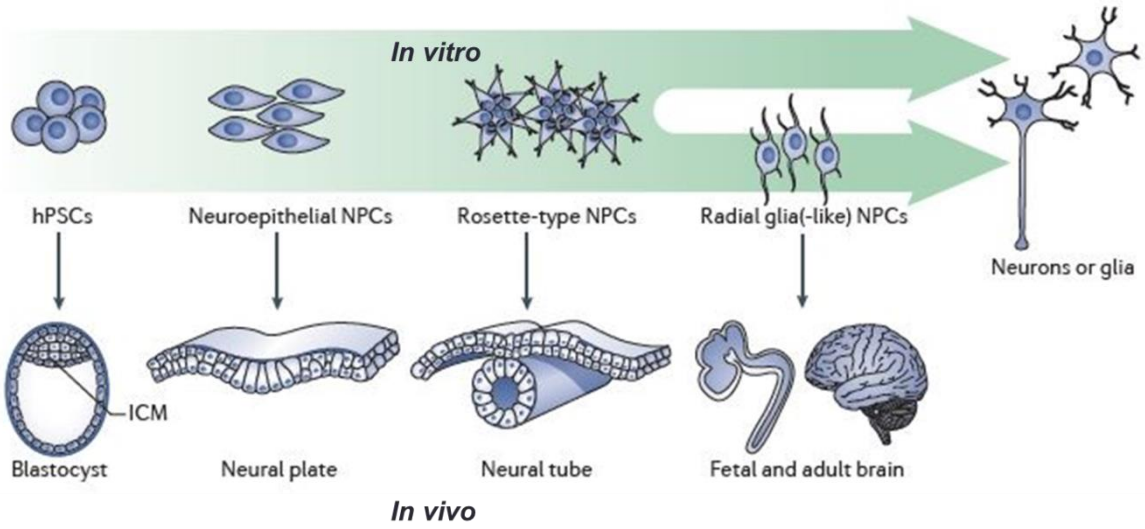

Figure I. 4 : Stages of neural differentiation *in vitro* and *in vivo*. When hPSCs differentiate into neurons *in vitro* (upper row), they transit through defined stages during which they resemble distinct NPC populations present during *in vivo* neurogenesis (lower row). hPSCs resemble the inner cell mass (ICM) of the blastocyst. hPSCs differentiate into neuroepithelial stem cells *in vitro*, corresponding to the neuroepithelial NPCs that form the neural plate *in vivo*. During *in vivo* neurulation, the neural tube closes, patterning along the developmental axes takes place and the first waves of neurons are generated. *In vitro*, the rosette-type NPCs that can also be derived from hPSCs resemble this developmental stage. During fetal and adult neurogenesis, radial glia gives rise to post-mitotic neurons. These correspond to the radial glia-like NPCs that are generated from the rosette-type NPCs *in vitro*. Adapted from [69].

I.3.3. Signaling pathways involved in hiPSC differentiation into neuroectoderm

The neural differentiation process has been recapitulated and studied *in vitro* since the arrival of hiPSC technology [72]. For this purpose, it is necessary to better understand the signaling pathways involved in this specific process [73].

A vital goal of stem-cell research is to identify the factors that will allow researchers to propagate and differentiate pure populations of stem cells [73]. Several signaling pathways known to control the fate of neural cells in the embryo were exploited to control the neural differentiation of ESCs, comprising Notch, Wnts, the FGF family and members of the TGF- β superfamily. The Notch pathway has arisen as an essentially important axis for controlling neural differentiation[74].
Several lines of evidence also demonstrate a crucial role of bone morphogenetic proteins (BMP) and Activin/nodal signaling inhibition during neural induction[75].

Activin and Nodal, members of the TGF-β superfamily, are also responsible for inducing mesendoderm, which is a precursor of endodermal and mesodermal lineages during the gastrulation process[75,76]. Besides TGF-ß proteins Activin and Nodal, TGF-β superfamily also includes growth

differentiation factors (GDFs) and BMPs, that inhibits the neuroectodermal path by promoting differentiation towards trophoblast through BMP-4 pathway [73].

I.3.3.1. Dual-SMAD inhibition protocol

As mentioned before, Activin and Nodal proteins mediate an important role inducing mesendoderm lineage [75]. Activin or Nodal can synergize with several other extracellular signaling proteins, more specifically FGF2 or WNTs, to promote stem-cell maintenance [73].

Small molecule inhibitors have proven extremely suitable for investigating signal transduction pathways[77]. By using a small molecule SB-431542, the Activin/nodal pathway is inhibited. This small molecule inhibits Lefty/Activin / TGFβ pathways by blocking phosphorylation of the ALK4, ALK5 and ALK7 receptors [75]. SB-431542 specifically inhibits the ability of activated ALK4, ALK5, and ALK7 to induce both Smad2/Smad4- and Smad3/Smad4-dependent transcription [77]. Since activation of SMAD 2/3 signaling is necessary for the maintenance of the undifferentiated state, inhibition of these two signaling pathways will allow the cells to begin the differentiation process by inhibiting the activing/nodal pathway [78,79].

Indeed, Chambers and his collaborators demonstrated that SB431542-mediated loss of pluripotency was associated with differentiation toward the trophoblast lineage. For this purpose they applied a Noggin/SB-431542 since Noggin is known to repress endogenous BMP signals that drive trophoblast fates upon differentiation and SB-431542 inhibits the Activin/nodal pathway, as previously cited [75] . Furthermore, they demonstrated that Noggin/SB-431542 protocol yielded an early $PAX6^{+}$ neuroepithelial population capable of rosette formation that represents the most primitive hESC – derived neural progenitor stage isolated to date. Taken together all this results revealed robustness and extension of the dual-SMAD-inhibition strategy beyond hESC differentiation[75].

With the purpose of inhibit the BMP signaling pathway, the addition of an antagonist, as dorsomorphin or the derivate LDN-193189 with higher specificity for BMP receptors, is essential [80]. This previous cited small molecule was more recently used for inhibiting BMP type I receptors ALK2 and ALK3 [73].
Thus, the dual-SMAD inhibition protocol is a procedure for the rapid commitment of confluent human PSCs into early PSC-derived neural precursors (NPs) [39].

The cells are first expanded in the right conditions to maintain the pluripotent state until they reach almost 100 % of confluence. Confluence is an important detail since initial cell density could affect lineage specification [39]. When dual-SMAD inhibition protocol is applied to cells at a lower density, the generated cells tend to be characteristic of peripheral nervous system (PNS), as neural crest stem cells rather than cells of the CNS. These later cells appear when a higher cell density is applied in the beginning of the differentiation protocol [75].

Culture conditions are also changed in order to include chemical inhibitors of BMP and Activin/Nodal signaling pathways, causing the emergence of a neuroepithelial cell sheet [39]. This induction is due to

the blocking of SMAD signaling transduction by SB- 431542 and LDN- 193189 small molecules [77,80] . When combined with basal N2B27 medium, these inhibitors repress mesoendodermal fates, directing the differentiation towards neuroectoderm. hiPSCs are induced into $PAX6^+$ NPs generating cells characteristic of CNS, that are morphologically organized into Neural rosette-like structures [39,76]. All of these features are summarized in figure I.5.

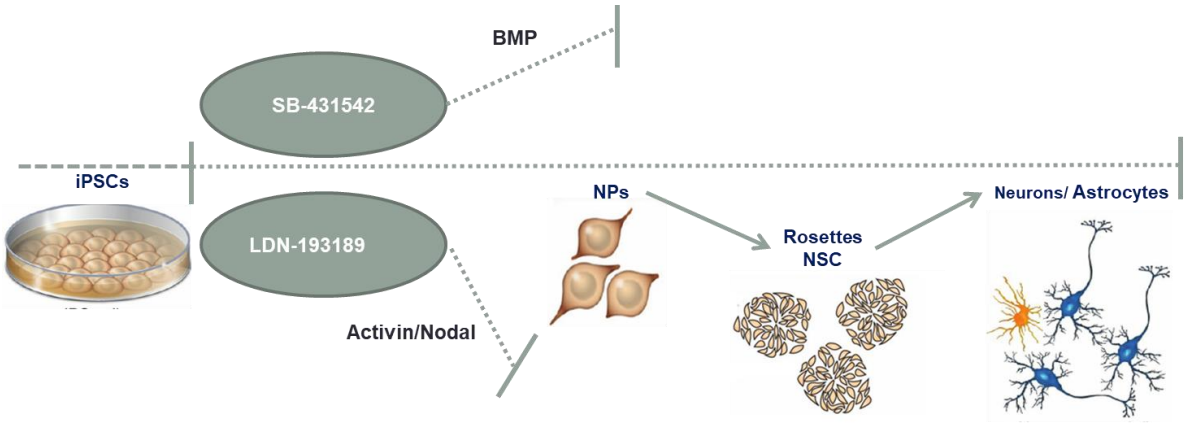

Figure I. 5 : Schematic view of dual-SMAD inhibition protocol for hiPSCs. Model for the mechanism of action of small molecules SB-431542, an inhibitor of mesendoderm lineage, and LDN-193189, an inhibitor of extra embryonic tissue.

I.3.4. Therapeutic methodologies using iPSCs

In 2006 the generation of iPSCs had a great impact in stem cell biology [33,42]. There are two interesting applications for hiPSCs; first, they are a robust source for regenerative medicine therapies and second, a powerful tool for the creation of human genetic disease modelling [81]. So far, many reports already exists showing that iPSCs were generated from a variety of patients and those iPSC-derived differentiated cells successfully reproduced the disease phenotypes, and this type of analysis provided the motivation for developing novel therapeutic approaches [81]. In particular, the advent of iPSC technology allows for the generation of patient-specific nervous tissue, which can be used to model a variety of neurological disorders [82].

Following the work accomplished in 2009 by Chambers, Fernandes and his collaborators performed the neural commitment of human PSCs under defined conditions and thus, allowing the recapitulation of neural development and the generation of patient- specific neural cells [75,39]. Therefore, their defined culture system provided a way to recapitulate some of the temporal and regional patterning events that occur during *in vivo* cortical neurogenesis [83]. Also, by deconstructing the natural complexity of neural development into a simpler experimental approach, they were able to mimic numerous aspects of Rett syndrome pathology, an X-linked neurodevelopmental disorder caused by mutations in the methyl-CpG-binding protein 2 (MECP2) gene, whose assists in the transcriptional silencing through DNA methylation [84]. Thus, these findings could potentially contributing to a better understanding of cortical development and disease [39].

In 2010, Chamberlain and his collaborators were able to create iPSCs models for AS and Prader–Willi Syndrome (PWS). Through this study it was discovered that iPSCs from normal individuals and from persons with AS and PWS presented the same methylation patterns as the fibroblast lines from which they were derived. A methylated maternal allele and an unmethylated paternal allele were both present in normal iPSCs, whereas only an unmethylated paternal allele was observed in AS iPSCs and only a methylated maternal allele was observed in PWS iPSCs, since these iPSC lines were originated from large deletions of the maternal or the paternal chromosome 15q11-13 region, respectively [85]. Nevertheless, these studies did not exposed very thorough analysis of the imprinting status. Thus, imprinting of *UBE3A* during neuronal differentiation from iPCSs remains unknown. Regarding that, human iPSC culture models of these and other human neurogenetic disorders will provide important tools to advance the understanding of disease mechanisms and to develop unique tools for drug discovery [85].

In 2017, Fink and his collaborators were able to generate iPSC-derived neurons from AS patients and healthy control subjects to examine the maturation of neuronal and synaptic activity in these cells. Their studies show that neurons derived from AS patients were similar to controls at initial time points, but exhibited deficits that were generally apparent by 6–8 weeks in vitro. Specifically, AS-derived neurons showed a more depolarized resting membrane potential (RMP), immature firing action potential (AP), decreased spontaneous excitatory synaptic activity and reduced capacity for activity dependent synaptic plasticity [86]. These phenotypic alterations were likely due to *UBE3A* loss during the neuronal differentiation, since *UBE3A* KO iPSCs also exhibit similar phenotypes. However, the authors did not address when and in which cells *UBE3A* silencing occurred and how this correlates with the timing of the defects they report. Obviously, this work was essential to show AS iPSCs can provide a cellular phenotype for further investigations of the specific role of *UBE3A* and its subsequent signaling mechanisms, and also for identifying and evaluating therapeutic strategies to mitigate the symptoms of AS and related neurodevelopmental pathologies [86]. It will be important to attempt different neuronal differentiation protocols to explore the full capacity of iPSC technology to study Angelman syndrome.

Nevertheless, the large number of studies since the original method that was published by Takahashi and Yamanaka [33] certainly demonstrates that these patient specific iPSCs offer a unique opportunity to mimic pathologic features *in vitro*, thus enabling disease investigation and drug development [87].

II. Aim of the Studies

One of the major innovations in regenerative medicine was the derivation of hiPSCs, which comprise unique features which allow them to be more accessible to several therapies in development, drug screening, research and disease modelling. Thus, by proceeding to the neural commitment of the Angelman-derived iPSCs we can mimic the neurogenesis process *in vitro*, which may be quite useful for the development of a model system for this disease.

This thesis work aimed at providing a robust disease modelling system, by using hiPSCs, to study Angelman Syndrome.
Specifically, two main objectives were defined:

1. Development of a human model system of Angelman Syndrome, through iPSCs neuronal differentiation with subsequent phenotypic characterization of the defects in AS hiPSC-derived neurons based on neuronal identity
2. Determination of the time and cell specificity for paternal *UBE3A* silencing during dual SMAD inhibition neurogenesis of hiPSCs.

III. Materials and Methods

III.1. Expansion of hiPSCs

III.1.1. Cell line

The iPSCs cell lines used in this project, WT-E and AS-D were reprogrammed from skin fibroblasts obtained either from a healthy individual or from an Angelman Syndrome patient, respectively. AS patient-derived iPSCs and WT patient-derived iPSCs were generated using lentiviral vectors encoding the reprogramming factors, Oct4, Sox2,Klf4 and Myc [16].

III.1.2. Adhesion substrate preparation

III.1.2.1. Matrigel®

Matrigel® (Corning®), which is a gelatinous protein mixture secreted by Engelbreth-Holm-Swarm mouse sarcoma, is rich in ECM molecules as laminin, entanctin and collagen IV, mimicking the complex extracellular environment found in many tissues. Matrigel® was stored in 200 µL aliquots at -20 ºC. The initial step of matrigel preparation includes the thaw of an aliquot on ice, at room temperature during about 60 minutes or overnight at 4 ºC. Next, matrigel was diluted in DMEM-F12® (1:60) (Gibco®) and the previously diluted solution was used to cover multiwall tissue culture plates (Falcon®). Afterwards, the covered plates were incubated at room temperature during a minimum period of two hours. If not used immediately, the covered plates can be stored at 4 ° C for approximately two weeks.

III.1.3. Culture media

III.1.3.1. mTeSR™1

mTeSR™1 (STEMCELL™ Technologies) is a highly specialized, complete, serum-free and defined formulation. mTeSR™1 is designed for the feeder-free maintenance and expansion of human embryonic stem cells (ES) cell) and human induced pluripotent stem cells (iPS cells) in the undifferentiated state. mTeSR™1 medium contains recombinant human basic fibroblast growth factor (rh bFGF), recombinant human transforming growth factor β (rh TGFβ). The addition of supplementary growth factors is not required. Nevertheless, the addition of 1:200 (v/v) dilution of penicillin/streptomycin (PenStrep, Gibco®) must be performed in order to prevent bacterial

contamination of cell cultures due to their effective combined action against gram-positive and gram-negative bacteria. mTeSR™ is compatible with Matrigel® as the culture matrix.

III.1.3.2. Washing medium

Washing medium formulation is used to maintain the cell cultures during some procedures in the laminar flow hood. Is also can be used for the inactivation of enzymatic activity. The formulation comprises DMEM/F12 (Gibco®) with L- glutamine, 2.44 g/L of sodium bicarbonate (SigmaAldrich) and was also supplemented with 10% Knockout-Serum replacement (KO-SR, Gibco®), 1% MEM- non essential amino acids (Gibco®) and 1% Pen/Strep (Gibco®). The medium was stored at 4ºC, and should reach room temperature before being used.

III.1.4. Culture of hiPSCs

III.1.4.1. Thawing hiPSCs

The hiPSCs were cryopreserved in cryovials (Thermo Scientific™) that were maintained in liquid nitrogen containers. In order to perform the thawing process it was necessary to pre warm to 37 ºC a 15 mL Falcon tube with 4 mL of washing medium, from which 1 mL was used to re-suspend the cells in cryovial. The cryovial was covered in gaze containing ethanol and place in a 37 ºC water bath. Afterwards was added drop-wise, 1 mL of washing medium that was pre-warmed before and then, the content of the cryovial was gently transferred to the previous Falcon tube containing washing medium. Next the tube containing the cell suspension was centrifuged (HERMLE Z 400 K) for 3 min at 1500 xg and the supernatant was then discarded and the pellet re-suspended in 1.5 mL of mTeSr1 medium. Finally the cell suspension was placed in 1 well of 6-well plate, pre-coated with Matrigel® and then the plate was incubated in a humidified incubator (Memmert), at 37 ºC with and 20 % of O_2 and 5 % of CO_2.

III.1.4.2. hiPSCs passaging with EDTA

Passaging using an EDTA-based dissociation solution can minimize cell death and allows for rapid cell attachment upon re-plating and resumption of the cell cycle [88]. Over time, this methodology enables rapid expansion of cell lines with minimal introduction of environmental and handling stresses. hiPSCs should be passaged when the colonies have reached their deal colony size without becoming overgrown, or when colonies have reached approximately 60 to 75 % confluency across the well. To start this procedure was necessary to aspirate the exhausted media and then each well was washed briefly with EDTA (Invitrogen™). Afterwards, each well was incubated with 1 mL of EDTA (0.5 mM) during 4 minutes, at room temperature. After this procedure EDTA was removed and the cells were rinsed and scraped from bottom with 2 mL of mTeSR™1 in order to collect the cells and then were

transferred to a 15 mL Falcon tube with additional medium according to the dilution wanted. Finally the cells were carefully re-suspended in order to not get single cells and were seeded in Matrigel-coated wells.

III.1.4.3. Cryopreservation of hiPSCs

To begin this procedure was necessary to wash each well briefly with EDTA (Invitrogen™). Afterwards, each well was incubated with 1 mL of EDTA (0.5 mM) during 4 minutes, at room temperature. After this, EDTA was removed and the cells were rinsed and scraped from bottom with 2 mL of mTeSR™1 and then were transferred to a 15 mL Falcon tube that was centrifuged during 4 minutes at 1000 xg. Then the supernatant was discarded and the pellet was re-suspended in 250 µL (per 2 wells) of freezing medium per vial, knowing that typically 2 wells of a 6-well plate were frozen in one vial. Freezing medium is composed by KO-SR containing 10% dimethylsulfoxide (DMSO; Gibco®). Each cryovial was filled with 250 µL of cell suspension, kept at – 80 °C for approximately 24 hours and finally was transferred to liquid nitrogen containers (– 196 °C).

III.1.5. Cell counting

In order to evaluate the cell viability and cell quantification it is necessary to add to the sample of cell suspension, a specific dye denominated Trypan Blue (Gibco®). This specific staining method allows the penetration of the membrane of dead cells that turn blue, which is not the case with living cells. First the exhausted media was removed from the well and was added 1 mL of accutase (Corning®), that is a natural enzyme mixture with proteolytic and collagenolytic enzyme activity that allows single cell detachment. Then, the plate was incubated for 7 min at 37 ºC and afterwards, to stop the action of accutase, 2 mL of washing medium was added. The cells suspension was centrifuged for 4 minutes at 1500 rpm and then the supernatant was discarded. Then the pellet was ressuspended in 0,5 mL of the appropriate culture media, taking into account the type of cells being counted. A volume of 10 µL of sample was collected, and mixed with 10 µL of trypan blue – 1:2 dilution. After thorough mixing by pipetting up and down, 10 µL of the resulting mixture were collected, placed into a haemocytometer, and counted under the optical microscope.

After the total cell count was obtained, cell concentration could be calculated from the subsequent equation:

$$Total\ cells/mL = \frac{total\ cells\ counted}{number\ of\ squares} \times dilution\ factor \times volume\ of\ sample \times 10^4 cells/mL \quad (1)$$

Is important to note that each square of the hemocytometer represents a total volume of 10^{-4} cm^3.

III.2. hiPSCs neural commitment

To start this protocol is necessary that the cells were maintained in a pluripotent state until they reached near 90-100 % of confluence. The neural commitment was performed by using N2B27 medium.

III.2.1. Neural induction of human iPSCs

The culture medium is composed by 50% (v/v) of N2 medium and 50% v/v of B27 medium. N2 medium consists in DMEM/F1(1:1)+Glutamax (Gibco®) supplemented with 1% (v/v) N-2 Supplement (Gibco®), 1.6 g/L of glucose (Sigma), 1% v/v PenStrep and 20 µg/mL Insulin (Sigma). B27 medium was formulated with Neurobasal® Medium (Gibco®) supplemented with 2% of B-27® Supplement (Gibco®), 2 mM of L-glutamine (Gibco®) and 0.5% of PenStrep. From day 0 to day 12 N2B27 medium was supplemented with 10 µM of SB-431542 (Stemgent™) and 100 nM of LDN-193189 (StemMACS ™).

III.2.2. Neuronal differentiation of human iPSCs

At day 12, human neural progenitors were passaged using EDTA (0.5 mM) and were re-plated in a split ratio of 1:3 into poly-L-ornithine (15 µg/mL; Sigma)-treated and Laminin (20 µg/mL, Sigma) coated plates. Between days 14 to 16, N2B27 medium was supplemented with bFGF-Basic fibroblast growth factor (10 ng/mL, Peprotech). At day 19, cells were again passaged by using EDTA, into new laminin-coated wells, in a split ration of 1:3. The medium was changed every two days, without the addiction of any small molecule or any factor. At day 27, cells were split with accutase and plated into laminin-coated wells at a density of 100.000 cells/cm^2 (300.000 cells per 12-well plate). The N2B27 medium was replaced every two days until day 70. At day 35 the medium was replaced by the Maturation N2B27 that contains some important neurotrophic factors that are essential for the neuronal maturation process. Maturation N2B27 was formulated with N2B27 that was supplemented with cAMP (0.5 mM, Sigma), Ascorbic Acid (0.2 mM, Sigma) and BDNF+GDNF (20 ng/mL, Peprotech). Until day 80, 50 % of the medium was changed every two days and cells were also supplement with laminin during this stage of the neuronal differentiation.

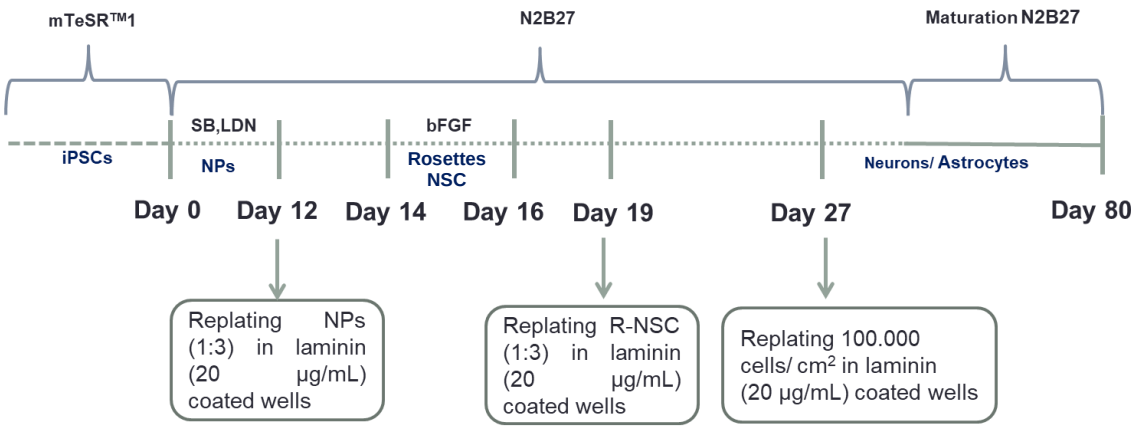

Figure III. 1 : Schematic view of neural and neuronal commitment steps: dual-SMAD inhibition by adding to the N2B27 medium SB – SB431542 and LDN – LDN193189 that inhibits Activin and Nodal and BMP pathways, respectively. During the neuronal differentiation, several replatings into laminin- coated wells were performed at days 12, 19 and 27.

III.3. Characterization of human iPSCs and hiPSCs- derived neural progenitors

III.3.1. Flow cytometry

The first step of this procedure was the removal of the exhausted medium from each well and then the cells were washed with 1 mL of PBS (Corning®). Afterwards, each well was incubated with 800 µL of accutase for 7 minutes at 37 ºC. The inactivation of accutase was performed by the addition of washing medium, being all the cells collected in a Falcon tube. The samples were then centrifuge for 4 min at 1500 xg, the supernatant was discarded and the pellet was resuspended with 2 % PFA in PBS. The samples were stored at 4 ºC.

III.3.1.1. Intracellular staining

The samples previously stored in 2 % (w/v) PFA were centrifuged (HERMEL Z 300 K) during 3 min at 1500xg and then washed twice with 1 % (v/v) normal goat serum (NGS, Sigma). Eppendorf tubes were initially coated with 1% (v/v) of BSA (Invitrogen™) in PBS for at least 15 min. Afterwards, the cells were re-suspended in 3 % (v/v) NGS and at least 5 x 10^5 cells per condition were transferred for pre-coated Eppendorf tubes (BSA was first removed). After transferring the same number of cells per condition, Eppendorf tubes were centrifuged at 1500xg during 3 min. Then the incubation with 1:1 of 3 % (v/v) NGS and 1 % (w/v) saponin (Sigma) were performed during 15 min at room temperature, for cell membrane permeabilization. Next, cells were washed with 3% NGS and the pellets of negative controls were re-suspended in 3 % (v/v) NGS only while the others were re-suspended with the primary antibody (in 3% NGS), during 1h at room temperature. Cells were then washed twice with 1 % (v/v) NGS and incubated in the dark, during 30 min, with the secondary antibody. After incubation, the

last washing procedure was performed, and the cells were re-suspended in PBS and transferred for FACS tubes. Afterwards the samples were analyzed in FACSCalibur™ flow cytometer (BD Biosciences®)and the results obtained were analyzed using Flowing Software 2.

III.3.1.1.1. Antibodies for intracellular staining

Oct4 (Milipore; 1:150), Sox2 (Sigma; 1200) and Goat anti-rabbit IgG Alexa Fluor – 488 (Life technologies; 1:500)

III.3.1.2. Surface marker staining

The samples previously stored in 2 % (w/v) PFA were centrifuge during 3 min at 1500xg and then washed with 2 mL of FACS buffer (4 % (v/v) FBS (ThermoFisher) in PBS). Then, approximately 5 x 10^5 cells per condition were re-suspended in 100 µL of FACS Buffer, including the negative controls. The primary antibodies were added in the recommended concentration in all of the samples with the exception of the negative controls and incubated for 15 min at room temperature, in the dark. Afterwards, the cells were washed twice with PBS and then re-suspended in FACS buffer. Then, the incubation with the secondary antibodies was performed, for 15 minutes, in the dark. Finally, the cells were washed twice with PBS, re-suspended in 300 µL of FACS Buffer and transferred for FACS tubes. Afterwards the samples were analyzed in FACSCalibur™ flow cytometer (BD Biosciences®) and the results obtained were analyzed using Flowing Software 2.

III.3.1.2.1. Antibodies for surface marker staining

Tra-1-60 (PE-conjugated, Miltenyi Biotec; 1:10), SSEA-4 (PE-conjugated, Miltenyi Biotec; 1:10) and Goat anti-rabbit IgG Alexa Fluor – 488 (Life technologies; 1:500)

III.3.2. Immunocytochemistry

III.3.2.1. Immunofluorescence staining of intracellular markers

The culture wells were washed with PBS and then the cells were fixed with 4% (v/v) PFA during 20 minutes. Afterwards, the cells were washed twice with 1 mL/well of PBS and then incubated with blocking solution (10 % (v/v) FBS and 1 % (v/v) Triton, in PBS) overnight or in alternative left for 60 minutes at room temperature. Primary antibodies were diluted in staining solution (5 % (v/v) NGS and 0.1 % (v/v) Triton, in PBS), added to the culture wells and left to incubate at 4ºC for 120 minutes. Afterwards, the cells were washed twice with 1 mL/well of PBS and then the secondary antibodies were also diluted in staining solution and incubated with cells during 60 minutes in the dark, at room temperature. The cells were washed 3 times with 1 mL of PBS/ well with the purpose of removing the

excess of secondary antibody and were left to incubate with 400 µL/well of 4',6-diamidino-2-phenylindole (DAPI), a fluorescent stain that binds to DNA, (diluted 1:10000 in $NaHCO_3$; Sigma-Aldrich) during 4 minutes in the dark, at room temperature. Finally, cells were washed with PBS to remove any DAPI crystals and left with PBS for further observation under fluorescence optical microscope (Leica Microsystems CMS GmbH, model DMI3000 B) or confocal microscopy (Leica TCS SP5 laser scanning microscope). For confocal observation, the coverslips were taken and by using Moviol, a mounting medium, they were assembled on blades. The images were treated using the Fiji-ImageJ software.

III.3.2.1.1. Antibodies for intracellular Immunocytochemistry

Primary antibodies: Pax6 (Covance, 1:400); Nestin (R&D, 1:400); Sox2 (Sigma, 1:200); β-III-tubulin (Tuj1, Covance, 1:4000); Glial Fibrillary Acidic Protein (GFAP, abcam, 1:100); NeuN (Cell Signaling Technology®, 1:200); *UBE3A* (Novus Biologicals 1:100); GAD65 (milipore, 1:100); VGAT (Santa Cruz, 1:100)

Secondary antibodies: Goat anti-mouse IgG Alexa Fluor – 488/546 (1:500); Goat anti-rabbit IgG Alexa Fluor – 488/546 (1:500).

III.4. RNA extraction and cDNA preparation

III.4.1. RNA isolation from Adherent cells (TRIzol Reagent)

To start this procedure it was necessary to remove the N2B27 medium from the cultured cells and then was added 1 mL of TRIzol Reagent (NZYtech) directly to the cells and finally the homogenized sample was incubated for 5 minutes at room temperature to allow complete dissociation of the nucleoprotein complex. Afterwards, the cell suspension was transferred to an Eppendorf tube, after pipetting up and down to destroy cell aggregates. If it was not intended to proceed with the procedure at the moment, the sample should be stored at – 80ºC until further use and thawed immediately before to proceed with the protocol. Then 0.2 mL of Chloroform per mL of TRIzol Reagent was added and after the addition the Eppendorf tube was shacked vigorously for 15 seconds. Afterwards, each sample was incubated for 2-3 minutes at room temperature and then centrifuged at 12000xg for 15 minutes at 4 ºC. Next, the aqueous phase that was formed was removed carefully avoiding the drawing of any of the interphase of the organic layer into the pipette and placed into a new Eppendorf tube. After that, 1 µL of Glycogen Blue (15 µg/ µL, Invitrogen™) was added, functioning as carrier to the aqueous phase. Next, 0.5 mL of 100 % Isopropanol was added to the aqueous phase and the samples were incubated for 10 minutes at room temperature and then centrifuged at 12000 xg for 10 minutes at 4 ºC. Afterwards, the supernatant was discarded and washed with 1 mL of cold 75 % (v/v) Ethanol. The samples were vortex briefly and then centrifuged at 7500 xg for 5 minutes at 4 ºC. Then the supernatant was discarded and the RNA pellet was kept to air dry for 10 minutes and re-

suspended in 30 µL of RNase-free water by pipetting the solution up and down in order to homogenize the cell suspension. Finally, the samples were quantified in Nanodrop 2000 (Thermo Scientific) and stored at -80 ºC until be used for the intended downstream application.

III.4.2. DNase Treatment of RNA samples

The first step of this procedure was the addition of RNase-free water to a final volume of 25 µL and 5 µg of RNA, to each Eppendorf tube. Then was also added to each Eppendorf tube 25 µL of DNase I mix2x that was composed, by 10x buffer (5 µL, Roche), DNase I (10µ/µL, 3.5 µL, Roche), RNase Out (1.1 µL, Bioline) and RNase-free water to equals the total volume of 25 µL, per each sample. Afterwards, the samples were incubated for 30 minutes at 37 ºC (Sanyo UNCUBATOR). Next, were added to each tube 5 µL (0.1x volume) of 3M Sodium Acetate (pH: 5.5) and 1 µL of Glycogen Blue. Then the precipitation occurred by adding to each sample 150 µL (3x volume) of 100 % Ethanol and next each tube was incubated at -80 ºC for at least 30 minutes. Afterwards, all the samples were centrifuged for 30 minutes at 13000 xg at 4 ºC, the supernatant discarded and the pellet washed with 1 mL of cold 70 % Ethanol. Then, a spin was made to each tube for 5 minutes at 4 ºC , the supernatant discarded and pellet was kept to air dry for 15 minutes and re-suspended in 10 µL of RNase-free water by pipetting the solution up and down in order to homogenize the cell suspension. Finally, the samples were quantified in Nanodrop and stored at -80 ºC until further use.

III.4.3. cDNA synthesis

cDNA synthesis was performed by using Transcriptor High Fidelity cDNA synthesis Kit (Roche) according to manufacturer's instructions. This procedure started with the addition at each 0.2 mL tube (frilabo) 500 ng RNA and RNase-free water up to 9.4 µL. Then was added to each tube, 2 µL of random primers (vial 6) and the tubes were left to incubate at 65 ºC on thermocycler (Applied Biosystems, Veriti 96 well Thermal Cycler) and cooled on ice for at least 5 minutes. Next was added to each Eppendorf tube 8.6 µL of RT mixture that was composed by RT buffer 5x (4 µL, vial 2), RNase Out 40 µ/µL (0.5 µL, vial 3), dNTPs mix 10 mM (2 µL, vial 4), DTT (1 µL, vial 7) and RT (1.1 µL,vial 1). Afterwards all the tubes were placed on thermocycler and incubated at 29 ºC for 10 minutes, then at 48 ºC for 60 minutes and finally at 58 ºC for 5 minutes. Then, all the tubes were stored at -20 ºC.

III.5. Quantitative real-time PCR Analysis (RT-qPCR)

Total RNA was isolated from cells at different stages of neural commitment (day 0, 17,28,37,64 and 80) as indicated in the section III.4.

cDNA was subjected to qPCR with iTaqTM SYBR® Green Supermix (Bio-Rad) in a ViiA7 Applied Biosystems machine according to the manufacturer's instructions for *PAX6, Oct4, NESTIN,* β-III-tubulin *(TUJ1), MAP2, UBE3A, SNORD115, GAD65, GAD67, VGLUT1* and *GAPDH* (primer

specifications are presented in table III.1). PCR reactions were run in duplicate, normalized to the housekeeping gene *GAPDH* and results analysed in QuantStudio™ Real-Time PCR Software.

Table III. 1 Primers used for RT-qPCR of cDNA samples

Primer	Forward	Reverse	Brand
hUBE3A	AGCCGGAATCTAGATTTCCA	TGTCTGTGCCCGTTGTAAACT	Sigma
hPAX6	GAATCAGAGAAGACAGGCCA	GTGTAGGTATCATAACTCCG	Sigma
hGAPDH	GAAGGTGGAGGTCGGAGTC	GAAGATGGTGATGGATTTC	Invitrogen™
hOCT4	GTGGAGGAAGCTGACAACAA	ATTCTCCAGGTTGCCTCTCA	Sigma
hMap2	GGCATTGAAGAATGGCAGAT	CCCTGTATGGGAATCCATTG	Sigma
hSNORD115	GTGTTGATGATGAGAACCTTATATTATCC	GGGCCTCAGCGTAATCCTATTG	Sigma
hNESTIN	GAAACAGCCATAGAGGGCAAA	TGGTTTTCCAGAGTCTTCAGTGA	Sigma
hVGLUT1	TACACGGCTCCTTTTTCTGG	CTGSGGGGATCAGCATGTTT	Sigma
hGAD65	GTCTCCAGCTCGCATACACA	CGAAAGACCAAAAGCCAGAG	Sigma
hGAD67	CCTGGAACTGGCTGAATACC	CCCTGAGGCTTTGTGGAATA	Sigma
hTUJ1	GCCTCTTCTCACAAGTACGTGCCTCG	GGGGCGAAGCCGGGCATGAACAAGAAGTGCAG	Sigma

III.6. Genomic DNA preparation from cultured cells

After the collection of the cell pellet, that was stored at -80 ºC until be used for the procedure, 500 µL of Lysis buffer with proteinase K was added to each sample and left to incubate overnight at 56 ºC (Thermo-Shaker, Grant-bio PHMT). The Lysis buffer was composed by 100 mM NaCl (Stock: 3M), 10 mM Tris pH 8.0 (Stock: 1M), 25 mM EDTA pH 8.0 (Stock: 0.5 M, Invitrogen™), 0.5 SDS (Stock: 10 %) and 0.2 µg/µL Proteinase K to be added fresh (Stock: 10 µg/µL, ThermoScientific). Next, 55 µL of 3M Sodium Acetate pH 5.2 and 500 µL of phenol:chloroform:isoamyl alcohol (Invitrogen™) was added to each tube and mixed vigorously by shaking. The samples were then centrifuged at maximum speed for 10 minutes at room temperature and then the top phase that was formed was carefully transferred avoiding the disruption or transferring of any organic phase or interface into the pipette and placed into a new Eppendorf tubes. Next, 500 µL of chloroform was added to the aqueous phase transferred in the previous step and then the samples were again centrifuged at maximum speed for 10 minutes at room temperature and the new top phase formed was transferred again into a new Eppendorf tube.

Afterwards, was added 450 µL of Isopropanol and the cells were left to incubate at -20 ºC for at least 60 minutes. Then, the Eppendorf tubes were centrifuged at maximum speed for 30 minutes at room temperature and the supernatant carefully removed. Next, 700 µL of 70 % ethanol was added gently to each tube that was centrifuged at maximum speed for 5 minutes at room temperature and the supernatant carefully discarded. Then, a short spin was performed in order to discard the remaining supernatant and next the pellet was kept to air dry for 15 to 30 minutes, re-suspended in 200 µL of RNase-free water by pipetting the solution up and down and left at 37 ºC for approximately 3 hours in order to homogenize the cell suspension. Finally, the samples were quantified in Nanodrop and stored at -20 ºC until be used for the intended downstream application.

III.7. Combined Bisulfite Restriction Analysis (COBRA)

DNA samples (500 ng) were bisulfite converted using the EZ DNA Methylation Gold Kit (Zymo Research) following manufacturer's guidelines. Afterwards, bisulfite treated DNA was amplified by nested PCR using the primers summarized in table III.2. Mix composition of the two PCR reactions are also summarized in table III.3.

The first amplification cycle conditions were 94ºC for 5min, then 35 cycles: 94 ºC for 50 sec, 51 ºC for 60 sec, 68 ºC for 60 sec, then 68 ºC for 10 min. Afterwards, 2 µL were then diluted into a fresh 50 µL reaction for the second amplification cycle which conditions were 94 ºC for 5 min, then 25 cycles: 94 ºC for 50 sec, 51 ºC for 60 sec, 68 ºC for 60 sec, then 68 ºC for 10 min.

Table III.2 Primers used for Nested PCR in bisulfite converted samples

Primer	Sequence	Brand
SNRPN DMR F1	GGTTTTTTTTTATTGTAATAGTGTTGTGGGG	Invitrogen™
SNRPN DMR F2	GGTTTTAGGGGTTTAGTAGTTTTTTTTTTTTAG	Invitrogen™
SNRPN DMR R1	CTCCAAAACAAAAAACTTTAAAACCCAAA	Invitrogen™
SNRPN DMR R2	CAATACTCCAAATCCTAAAAACTTAAAATATCTA	Invitrogen™

Table III.3 Mix composition for Nested PCR in bisulfite converted samples

Mix composition	PCR 1 (µL)	PCR 2 (µL)
dH2O	38.5	37.5
10x Buffer	5	5
dNTP´s	1.5	1.5
SNRPN DMR F1	1.75	1.75
SNRPN DMR F2	1.75	1.75
SNRPN DMR R1	-	1.75
SNRPN DMR R2	-	1.75
NZlong (NZYTech)	0.5	0.5
DNA	1	2

For COBRA, PCR products were purified from enzymatic reactions using the NZYGelpure kit (NZYTech) and then submitted to a restriction enzyme digestion using the FastDigest Bsh1236I restriction enzyme (ThermoScientific), to distinguish methylated from unmethylated alleles based on the original status of the CGCG sequence, according to the manufacturer's instructions, but increasing the digestion time to 1 hour.

Digestion products were separated on a 2 % (w/v) agarose gel in 1X TAE in the presence of the 1 Kb Plus DNA ladder during approximately 20 minutes at 70 V. Digital images were obtained using the Chemidoc XRS+ system (BioRad) and analyzed using the Image Lab 5.2 software (BioRad).

III.8. Statistical Analysis

Results are present as standard error of the mean (SEM) and the statistical analysis was performed using two-tailed nonparametric tests, as *t*-test for independent samples. When statistical analysis was applied, at least two independent samples were evaluated. A p-value less than 0.05 were considered statistically significant.

IV. Results and Discussion

IV.1. Characterization of Angelman-derived and control iPSCs

To demonstrate the pluripotency state of both control and Angelman-derived iPSC lines, a flow cytometry analysis was performed for the main pluripotency markers (SSEA4 and TRA-1-60 - surface markers and OCT4 and Sox2 - intracellular markers). As expected, both control and Angelman-derived iPSCs expressed these four markers in the majority of the cells (always over 80% or more) as determined by flow cytometry-quantitative analysis (figure IV.1 and figure IV.2).

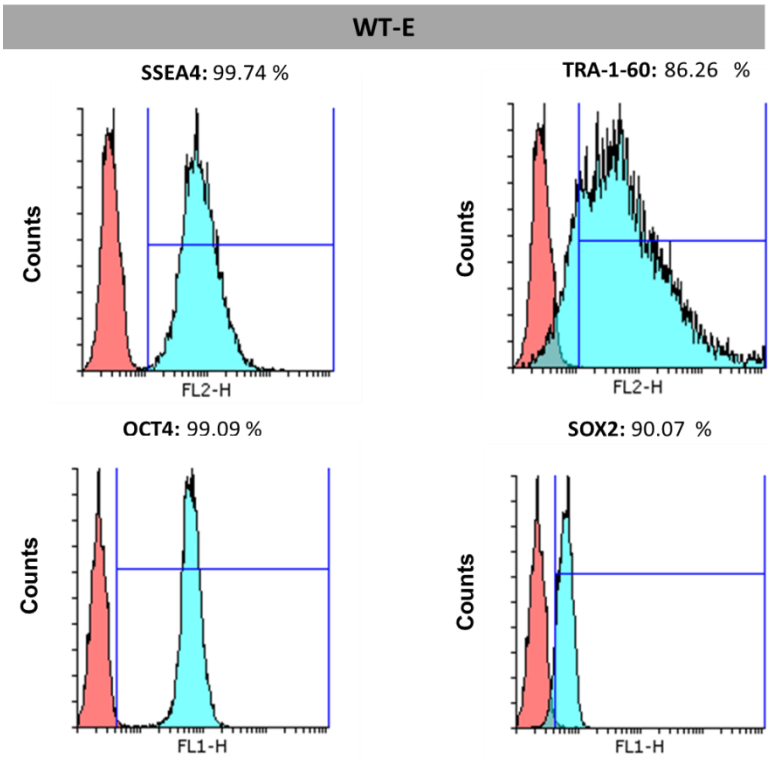

Figure IV. 1 : Expression of the pluripotency intracellular and extracellular markers in control iPSCs (WT-E): SSEA-4, TRA-1-60, OCT4 and SOX2. The quantitative results represent the positively stained percentage of cells analyzed by flow cytometry (FC). The red area in each FC graph represents the negative control and the blue area represents the stained cells.

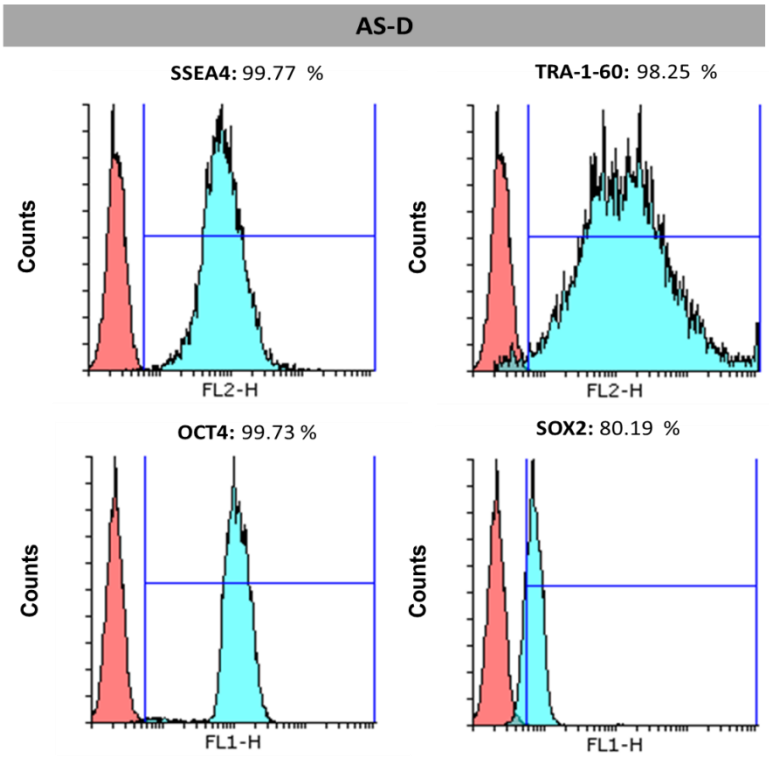

Figure IV. 2 : Expression of the pluripotency intracellular and extracellular markers in Angelman-derived iPSCs (AS-D): SSEA-4, TRA-1-60, OCT4 and SOX2. The quantitative results represent the positively stained percentage of cells analyzed by flow cytometry (FC). The red area in each FC graph represents the negative control and the blue area represents the stained cells.

Indeed, high percentage of hiPSCs was found to express the main pluripotent-associated surface markers. More specifically, for SSEA-4, a stage-specific embryonic antigen, the populations expressing this marker were approximately 99 % for either the control and Angelman-derived iPSCs (figure IV.1). Also for OCT4 and TRA-1-60 the same behavior was observed, but with a more pronounced difference for TRA-1-60 (86.26 % versus 98.25 % for the control and Angelman-derived iPSCs, respectively), in terms of percentage of expression (figure IV.1 and figure IV.2). For SOX2, there was a more pronounced difference between the two cell-lines, with a lower percentage of expression of this pluripotency marker seen in Angelman-derived iPSCs (80.19 %) when compared to control iPSCs (90.07 %) (figure IV.1 and figure IV.2). Taken together, these results indicate a pluripotent state of these iPSC populations before initiation of the neural commitment protocol.

IV.2. Neuronal Differentiation

The neuronal differentiation procedure was performed using the dual-SMAD inhibition protocol, combining both inhibiting small molecules, SB-431542 and LDN-193189, with N2B27 medium, which has been proven to be an efficient protocol for inducing hiPSCs into PAX6+ Neural progenitors generating cells characteristic of CNS [39,73,75]. To start this procedure cells need to be maintained in a pluripotent state until they reached near 100 % of confluence. At day 0, N2B27 medium was added in combination with the two small molecules, LDN and SB until day 12. Between days 13 to 16, N2B27 medium complemented with bFGF was used. bFGF is a growth factor with the ability of promoting proliferation of neural progenitors and thus allowing the formation of neuroepithelial rosettes that mimics the process of neural tube formation *in vivo* and appear after replating in laminin coated surfaces [70]. Maturation started at day 35 with the replacement of N2B27 medium by the Maturation N2B27 that contains some important neurotrophic factors (BDNF, GDNF, cAMP and ascorbic acid) that are essential for the neuronal maturation process.

IV.2.1. Generation of patient-specific neural progenitors

In this section, the aim was to confirm the expression of the neuroectoderm and specific differentiation markers by RT-qPCR and immunofluorescence (IF) staining from day 0 to day 37. The figure IV.3 illustrates the gene expression profile of some markers namely *OCT4*, a marker of pluripotency, the typical progenitor markers PAX6 and NESTIN and the neuronal marker beta III-tubulin (TUJ1). RT-qPCR analysis revealed expression of *OCT4* mainly at day 0, as expected since during the neural commitment protocol cells start to acquire a more committed phenotype, losing the pluripotent capacity and consequently, the expression of pluripotency genes [89]. RT-qPCR results also showed that both cell-lines WT-E and AS-D expressed neural markers, such as PAX*6* and NESTIN and the neuronal marker for newborn immature neurons *TUJ1*, which starts to rise at day 17 and more pronouncedly around day 28 to 37.In order to verify qualitatively the formation of neural progenitors along the neural induction, IF was performed for different markers. Figure IV.4 shows the direct iPSCs differentiation towards neuroectoderm that was confirmed by the expression of PAX6 and NESTIN*,* which are mainly expressed in the early stages of neural induction. Around day 17, it was possible to identify neural rosettes staining for SOX2, which is a NPs marker. In addition, TUJ1 was expressed since day 28 together with a visible reduction of PAX6, at this stage.

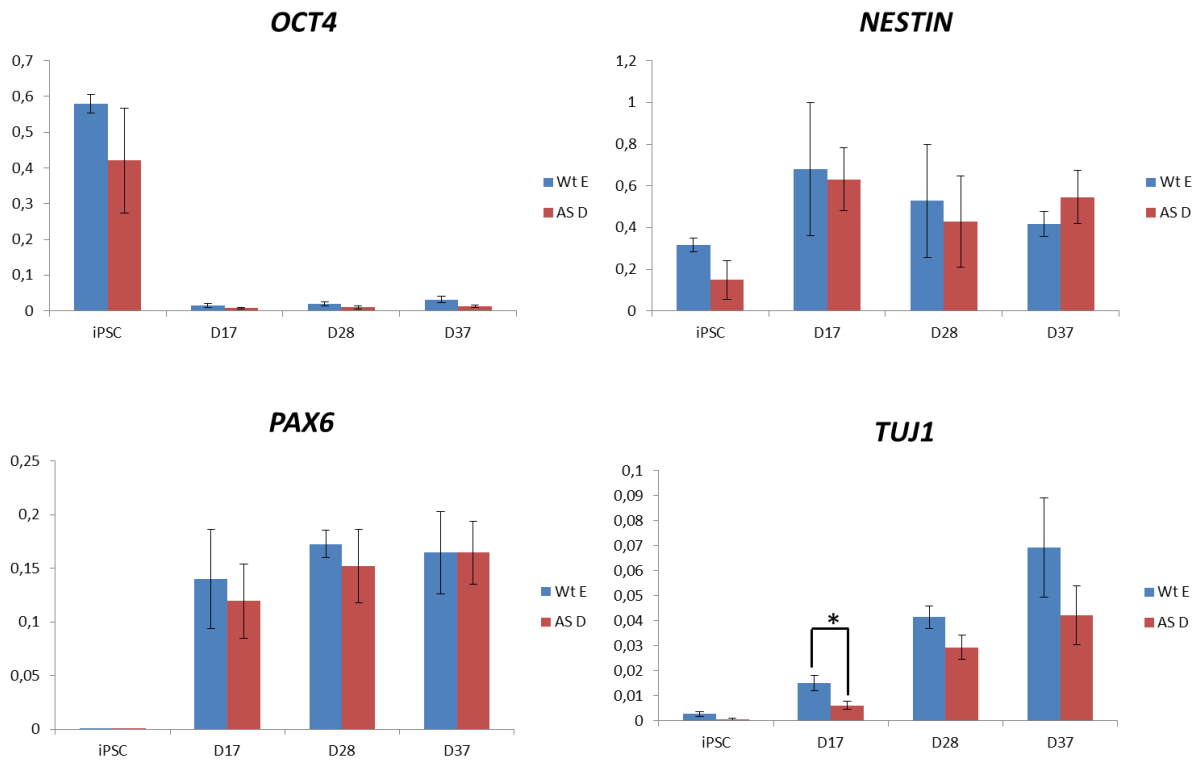

Figure IV. 3 : Expression of pluripotency marker *OCT4*, typical neural markers (NESTIN and PAX6) and of neuronal marker *TUJ1*, accessed by quantitative real-time PCR (RT-qPCR) at different stages of neural differentiation. Results are presented in this figure as standard error of the mean (SEM) and were all normalized for GAPDH housekeeping gene. * indicate statistical significance (P-value < 0.05)

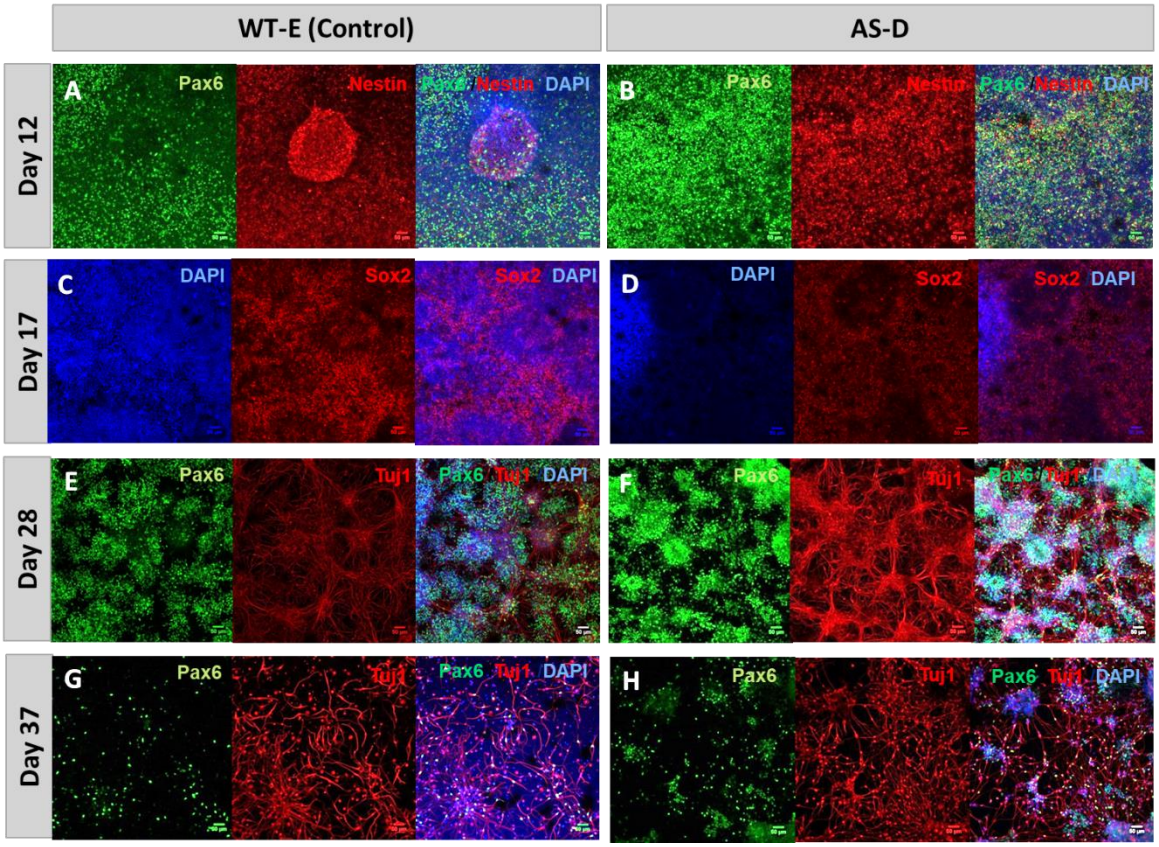

Figure IV. 4 : Confocal microscopy images of immunofluorescence staining for control (WT-E) and Angelman (AS-D) derived from human iPSCs at different stages of the neural commitment protocol using N2B27 medium and laminin-coated surfaces. A, B - At day 12 of differentiation, immunostaining analysis was performed for the typical neural progenitor markers Pax6 and Nestin either in control and Angelman-derived cells (scale bars: 50 µm). C, D- At day 17 cells were marked for Sox2 to identify neural rosettes either in control and Angelman-derived cells (scale bars: 50 µm). E, F, G, H - At days 28 and 37 cells were marked also with neural marker Pax6 and the neuronal marker Tuj1 with evident Tuj1- positive neuronal projections either in control and Angelman-derived cells (scale bars: 50 µm). Total cells were stained with DAPI and the images obtained with immuno- and DAPI staining were merged together (Scale bars – 50 µm).

Taking into account the previously showed results is possible to see that on day 12, the expression of typical early neural progenitor markers PAX6 and NESTIN, a sort of intermediate filament protein which is transiently expressed in adult NSCs and immature neural progenitor cells, appears in both cell lines in almost the same extent [90]. The majority of cells were indeed positive for PAX6 complemented with NESTIN positive cells either in control and Angelman-derived cells (figure IV.4A and 4B). At day 17, SOX2 staining revealed the presence of neural rosette structures on both conditions (figure IV.4C and 4D).

From around day 28 of differentiation, TUJ1-positive immature new born neurons outgrew from neural rosettes in addition to the nuclear neural progenitor co-staining for PAX6 (figure IV.4E and 4F), as suggested by Fernandes *et al* [39].

At day 37, it was possible to see that the expression of the typical early neural progenitor markers decreases in comparison with day 28, as expected since in this stage the neural progenitors give rise to more mature neurons (TUJ1-positive neurons could be identified) (figure IV.4G and 4H) [58].

Likewise, after peaking during the initial stage of commitment, expression of typical neural markers (PAX6 and NESTIN) declined during further differentiation and a progressive appearance of the neuronal marker TUJ1 starts to occur. It is also possible to see that comparing both control and Angelman-derived cell lines, that this one presented significantly more cell density along all the differentiation process with more proliferative capacity in comparison with control. Taking together, the results obtained for these markers by immunofluorescence (figure IV.4) and the expression profiles acquired by RT-qPCR (figure IV.3) proved that the neural induction was well succeeded, since results for both cell lines were very similar and coherent with previously obtained results.

IV.2.2. Neuronal maturation of control and Angelman-derived neurons

Neuronal maturation begun at day 35 and finished at day 80 with the replacement of N2B27 medium by the Maturation N2B27, as previously described. The purpose of this stage was to confirm if neuronal maturation was occurring in an efficient manner and if there were significant differences in morphology, proliferation and expression of markers characteristic of maturing neurons, either for control and Angelman-derived neurons. For this purpose, several IF staining analysis and expression analysis by RT-qPCR were performed from day 0 to day 80. The figure IV.5 illustrates the gene expression profile of some markers namely *MAP2*, a neuronal marker specifically expressed in dendrites of neuronal cells, *VGLUT1*, a vesicular transporter selectively expressed in functionally subpopulations of glutamatergic neurons and *GAD65* and *GAD67*, two similar markers expressed in GABAergic neurons[63]. By IF analysis, neural markers GAD65 and VGAT expression levels were evaluated at days 64 and 80 of neuronal differentiation for control and Angelman-derived neurons (figure IV.6).

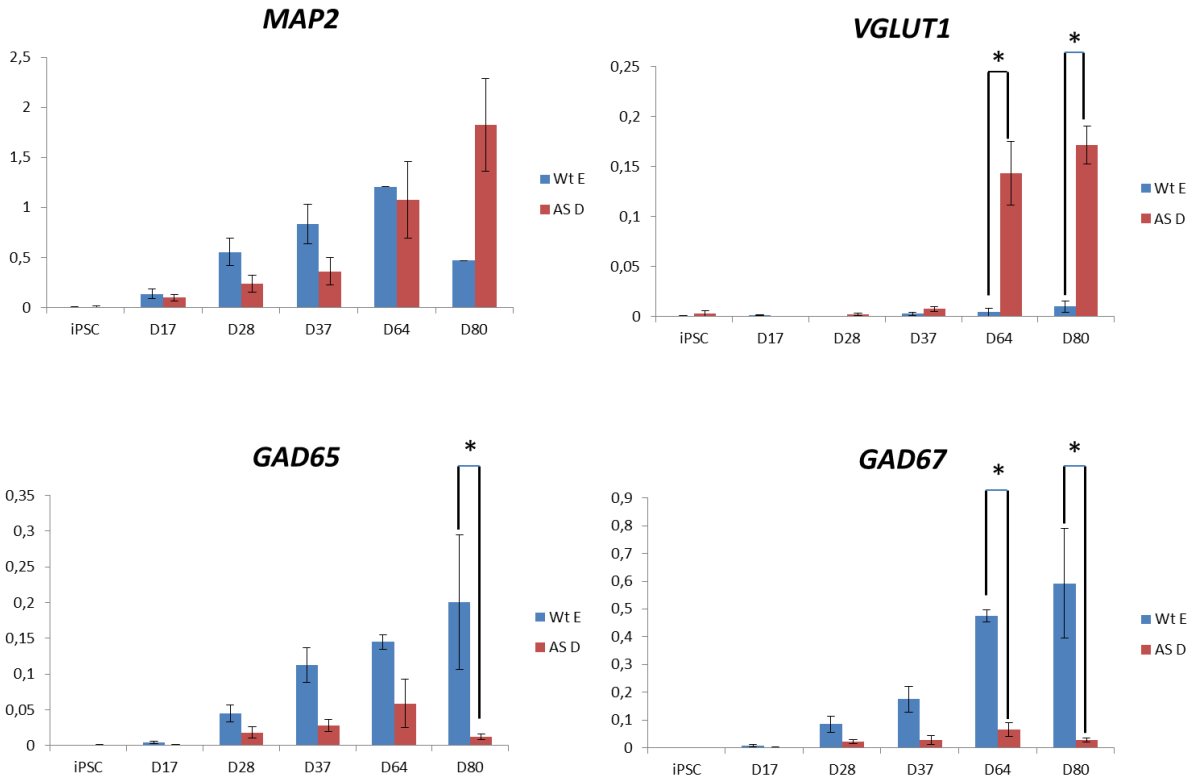

Figure IV. 5 : Expression of maturation markers (*MAP2*, *VGLUT1*, *GAD65* and *GAD67*) accessed by quantitative real-time PCR (RT-qPCR) at different stages of neural differentiation. Results are presented in this figure as standard error of the mean (SEM) and were all normalized for GAPDH housekeeping gene. * indicate statistical significance (P-value < 0.05)

RT-qPCR analysis revealed an increase in expression of *MAP2*, along the neuronal differentiation process, which started to appear at day 17, but raised from day 28, with a more pronounced, but not statistically significant, increase in control in comparison with Angelman-derived neurons. RT-qPCR results suggest a majority of Glutamatergic neurons for Angelman-derived neurons, since expression of *VGLUT1* is strongly upregulated only for AS-D at day 64 and day 80, a finding not observed for the WT-E control neurons. Instead, the control WT-E cell line showed an increase of *GAD65* and *GAD67* expression compared to the AS-D neurons, consistent with the presence of a majority of GABAergic neurons in the WT-E line (figure IV. 5).

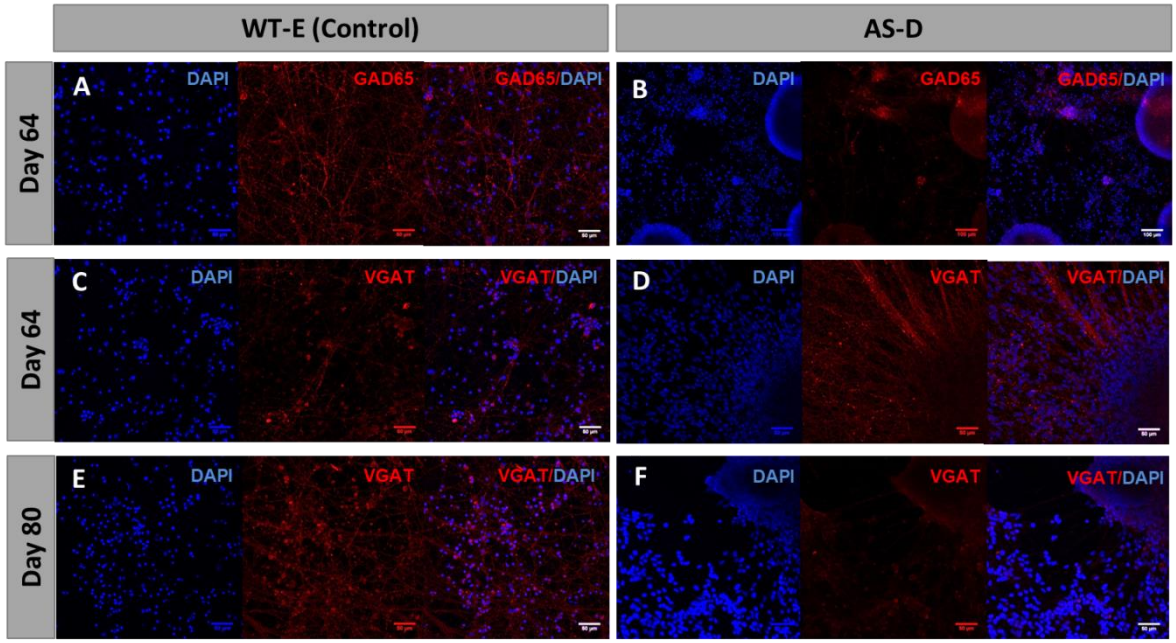

Figure IV. 6 : Confocal microscopy images of immunofluorescence staining for control (WT-E) and Angelman (AS-D) derived from human iPSCs at different stages of the neural commitment protocol using N2B27 medium and laminin-coated surfaces. A, B - At day 64, immunostaining analysis was performed for the detection of GABAergic interneurons (evident GAD65-positive neuronal population) and DAPI either in control and Angelman-derived cells (scale bars: 50 µm and 100 µm, respectively). C, D, E, F - At days 64 and 80 cells were marked with DAPI and the GABAergic marker, VGAT either in control and Angelman-derived cells (scale bars: 50 µm). Total cells were stained with DAPI and the images obtained with immuno- and DAPI staining were merged together (Scale bars – 50 µm and 100 µm).

Consistent with RT-qPCR expression, it is possible to see that on day 64, the neuronal cells were prevalently GAD65 positive in control in comparison with Angelman-derived neurons in which the expression is absent for this marker (figure IV. 6A and IV. 6B). The same behavior could be observed for the VGAT staining at days 64 and 80, in which a substantial fraction of neurons were positive for VGAT at day 64 in control comparatively to a decreased and more heterogeneous expression of this marker in Angelman-derived neurons (figure IV. 6C and IV. 6D). In addition, there was a significant increase in expression of this marker at day 80 that was only detectable in control-derived neurons (figure IV. 6E and IV. 6F). In future analyses might be advantageous the use of specific markers for glutamatergic neurons either by IF or RT-qPCR to validate the RT-qPCR results for vGLUT1 in Angelman versus control neurons.

In contrast, previous studies by Fink *et al* did not showed significant differences in terms of glutamatergic or GABAergic neuron proportions, between control and AS cultures [86]. Furthermore, previous studies showed that GABAergic inhibitory neurons appear to be more sensitive to pathological factors (*e.g*. ischemia, epilepsy and schizophrenia) in comparison with glutamatergic neurons [91]. Regarding that, down-regulation of GABAergic neurons in the Angelman differentiation could be due to an unknown brain dysfunction triggered by this disease which might result in the functional impairment of these GABAergic neurons. Future work must also be focused in the performance of several tests to confirm this hypothesis.

IV.2.3. Morphological features and cellular density in Control versus Angelman-derived iPSCs

During neuronal differentiation some morphological characteristics were particularly noticeable different between control and Angelman-derived iPSCs. Some qualitative analysis was performed to dissect these specific differences in terms of cell density and cellular morphology. Figure IV.7 displays representative images of DAPI staining (a DNA marker which highlights the nuclei of the cells) and Brightfield views of both control and Angelman iPSC-derived neurons at day 64 of neuronal differentiation.

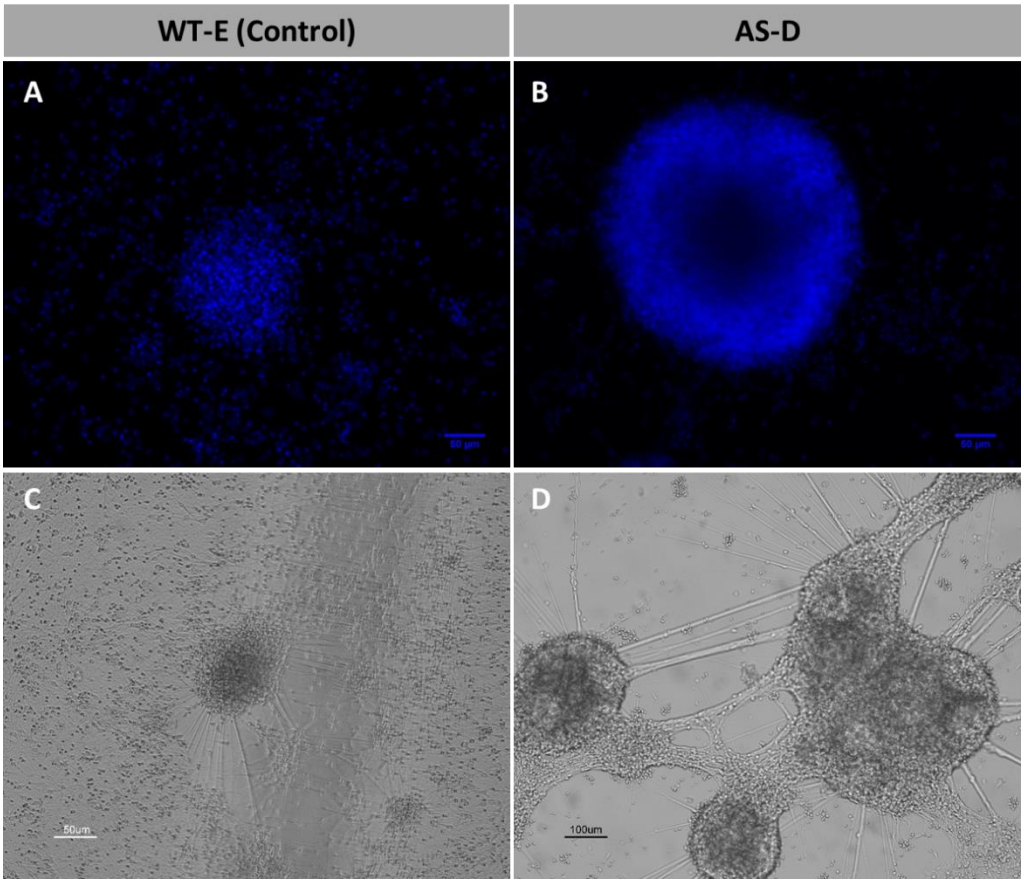

Figure IV. 7 : Confocal microscopy and Brightfield images of immunofluorescence staining for control (WT-E) and Angelman (AS-D) derived from human iPSCs at day 64 of neural commitment protocol using N2B27 medium and laminin-coated surfaces. A, B - At day 63 of differentiation, nuclear staining for DAPI was performed either in control and Angelman-derived cells (scale bars: 50 µm). C, D - Brightfield image at day for control (scale bar: 50 µm) and Angelman-derived cells (scale bar: 100 µm).

For the control neurons, a widespread neuronal population with small aggregates in the middle with a rounder shape arrangement was observable (figure IV. 7A and IV. 7C). In marked contrast, Angelman iPSC-derived neurons have substantial more aggregates that presents higher diameters (figure IV. 7B). These formed aggregates were not uniform in comparison with each other and were all interconnected between them (figure IV. 7D). This increase in the number of neurons and neuronal networks in Angelman neurons was the most notorious phenotype observed in our experiment. This phenotypic differences observed in this AS model can be used as a good starting point to better understand the physiological abnormalities of AS patients.

IV.2.4. *UBE3A* expression during neuronal differentiation

It is widely known that the paternal *UBE3A* allele will eventually become silenced in neurons. However, it is not known when this event occurs during development. For our neuronal differentiation to be a good model for AS, the paternal UBE3A allele should gradually be repressed along the process. The rationale of this section was to understand whether within the time-frame of our study, paternal *UBE3A* will become silenced in neurons. For that, we evaluate *UBE3A* expression by both IF staining and also RT-qPCR analysis from day 0 to day 80 of neuronal differentiation. Along with *UBE3A*, we also assess the upregulation of the paternal *SNORD115* snoRNA by RT-qPCR analysis. This gene is supposed to be expressed only in neurons and to match the expression of the *UBE3A-ATS*, which is involved in the silencing of the paternal *UBE3A* gene.

IV.2.4.1. Evaluation of methylation status of PWS-IC region by COBRA

To understand whether the normal imprinting pattern of the Angelman locus was maintained through dual SMAD-induced neuronal differentiation, the methylation pattern of the PWS-IC region of chromosome 15q11-q13 (figure IV.8A) was studied in Control and Angelman-derived cells at three timepoints: the beginning (day 0), intermediate (day 37) and last time point (days 80) by COBRA (figure IV.8B). We analyzed two independent biological replicates at day 37 and day 80 for AS-D and WT-E cells.

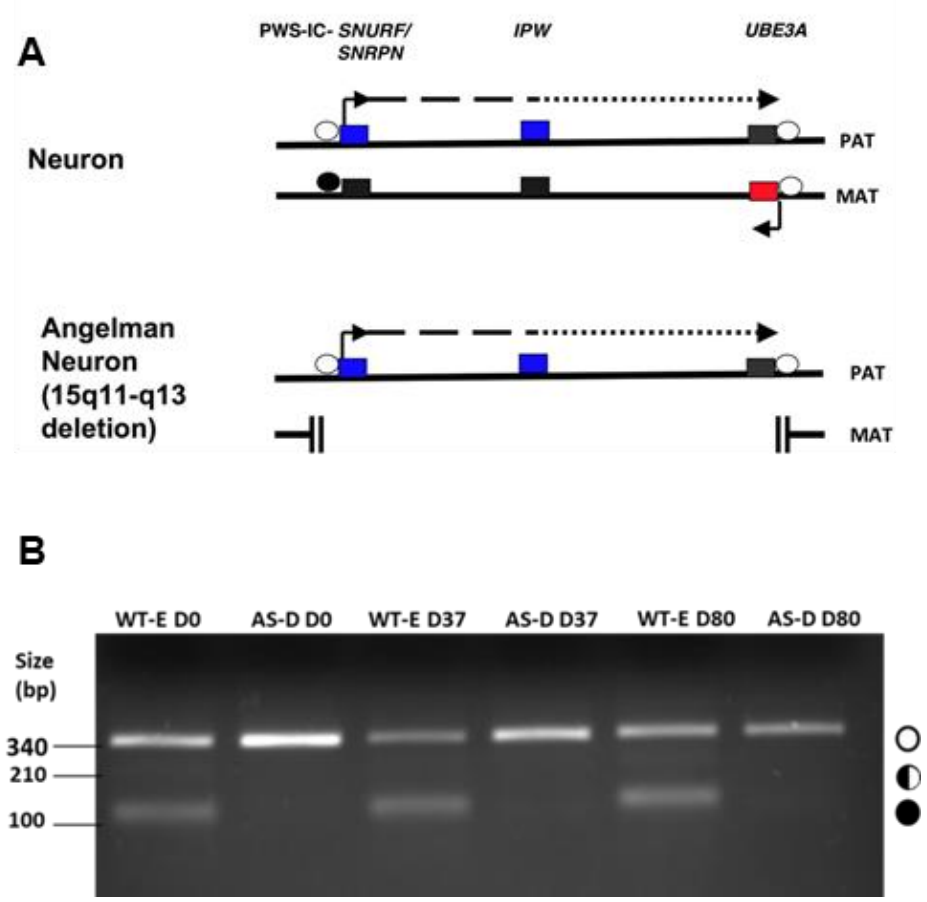

Figure IV. 8 : A - Genomic imprinting of chromosome 15q11-q13 and epigenetic silencing of *UBE3A* in neurons. In neurons, the paternal long noncoding RNA extends to and overlaps *UBE3A* as an antisense (*UBE3A-ATS*) with correlated silencing of the paternal *UBE3A* allele. In neurons from AS 15q11-q13 deletion patients, there is no active copy of *UBE3A* due loss of the maternal allele. Blue rectangles represent imprinted transcripts that are paternally expressed, red rectangles represent imprinted transcripts that are maternally expressed and black rectangles represent the repressed alleles of imprinted genes. White circles– unmethylated PWS-IC; black circles –methylated PWS-IC. Adapted from [92] **B -Characterization of the imprinting status of the chromosome 15q11-q13 region PWS-IC COBRA for WT-E (control) and AS-D in days 0, 37 and 80.** White circles– unmethylated band; half black circles – partially methylated band; black circles – fully methylated band.

Angelman-derived cells (AS-D) only displayed an unmethylated allele throughout neuronal differentiation in the two biological replicates. This corresponds to the PCR amplicon which was not cleaved by the restriction enzyme used in the assay and corresponds to the single paternal allele, since the maternal region is inexistent in these cells. In contrast, in control cells (WT-E) from the healthy donor at any of the stages analyzed for the two biological replicates, we could detect several bands that correspond to fully methylated (~100 bp), a weak partially methylated (~210 bp) and unmethylated (~340 bp) alleles (figure IV.8). The unmethylated band might correspond to the paternal allele, while both fully and partially methylated bands could correspond to the maternal allele, as indicated by Pólvora *et al* [16] . The results obtained were in accordance with the ones obtained by Pólvora *et al*, in control and Angelman-derived iPSCs[16]. More importantly, these results indicate that the imprinting status is maintained during the neuronal differentiation of such iPSCs, which suggests that this could be a robust disease modelling platform to study Angelman syndrome.

IV.2.4.2. Paternal *UBE3A* is partially repressed during *in vitro* neurogenesis of Angelman-derived iPSCs

In addition to the maintenance of the PWS-IC methylation status during neuronal differentiation, the other essential feature of a suitable AS model is the gradual repression of the paternal UBE3A allele along the differentiation process [85].

In order to check whether this repression was more pronounced along the differentiation protocol and particularly to discover when the paternal *UBE3A* imprinting occurs, IF staining and RT-qPCR analysis were executed from day 0 to day 80. Figure IV.9 illustrates the expression profiles of several markers like *UBE3A* and the neuronal-specific paternally expressed SNORD115 gene by RT-qPCR.

By immunocytochemistry analysis, the expression of *UBE3A* was evaluated at several stages of neuronal differentiation with the co-staining for specific markers characteristics of each time-point as *PAX6*, an early neural progenitor marker, NeuN protein that is located in nuclei and perinuclear cytoplasm of most of the neurons in the CNS and glial fibrillary acidic protein (GFAP), an astrocyte marker [93]. These immunocytochemistry results obtained for neuronal differentiation analysis are represented on Figure IV.10 and IV.11.

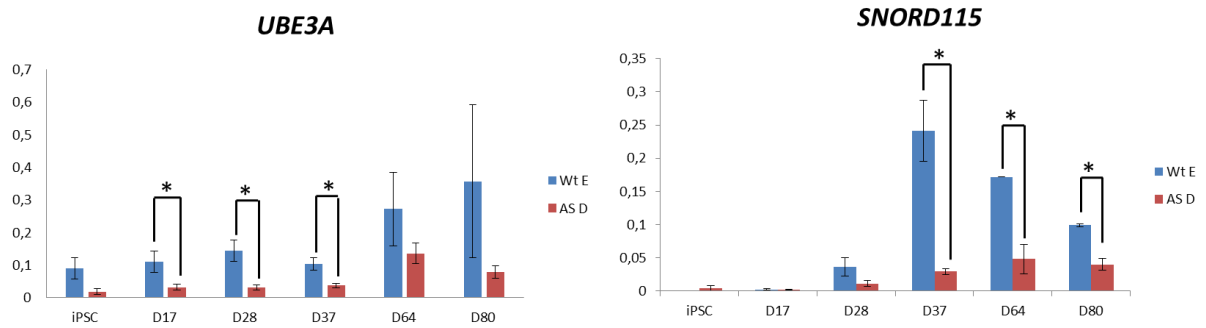

Figure IV. 9 : Expression of *UBE3A* and Snord 115 accessed by quantitative real-time PCR (RT-qPCR) at different stages of neural differentiation. Results are presented in this figure as standard error of the mean (SEM) and were all normalized for GAPDH housekeeping gene. * indicate statistical significance (P-value < 0.05)

RT-qPCR analysis revealed an increase in *UBE3A* expression along the neuronal differentiation process, with a more pronounced increase in control in comparison with Angelman-derived neurons, as expected since control has two *UBE3A* copies, while AS only have one. As for AS-D, the same expression profile is maintained along the differentiation meaning that at day 80, *UBE3A* is not totally repressed and *UBE3A* silencing did not yet occur in later stages of neuronal differentiation used in our study (figure IV.9).

RT-qPCR results also showed that on day 0, there is no expression of *SNORD115* gene for both cell lines, as expected since *SNORD115* expression is restricted to iPSC-derived neurons[85]. *SNORD115* expression starts to increase around day 28 of the neuronal differentiation reached its peak at day 37, for the control. After day 37, *SNORD115* expression undergoes a gradual decrease that is maintained until day 80, for the control. Unexpectedly, the expression of *SNORD115*, which is expressed exclusively from the paternal allele, was found markedly reduced in AS-D from day 37 of differentiation when compared to the control (figure IV.9). Since the methylation on the paternal unmethylated PWS-IC is not different in control versus AS-derived iPSCs, we were expecting to see comparable levels

between the two iPSCs. The reasons behind such a difference are difficult to explain. One possibility is that *SNORD115* levels of expression are higher in GABAergic neurons which are underrepresented in AS-D neurons. This possibility will need to be confirmed in the future.

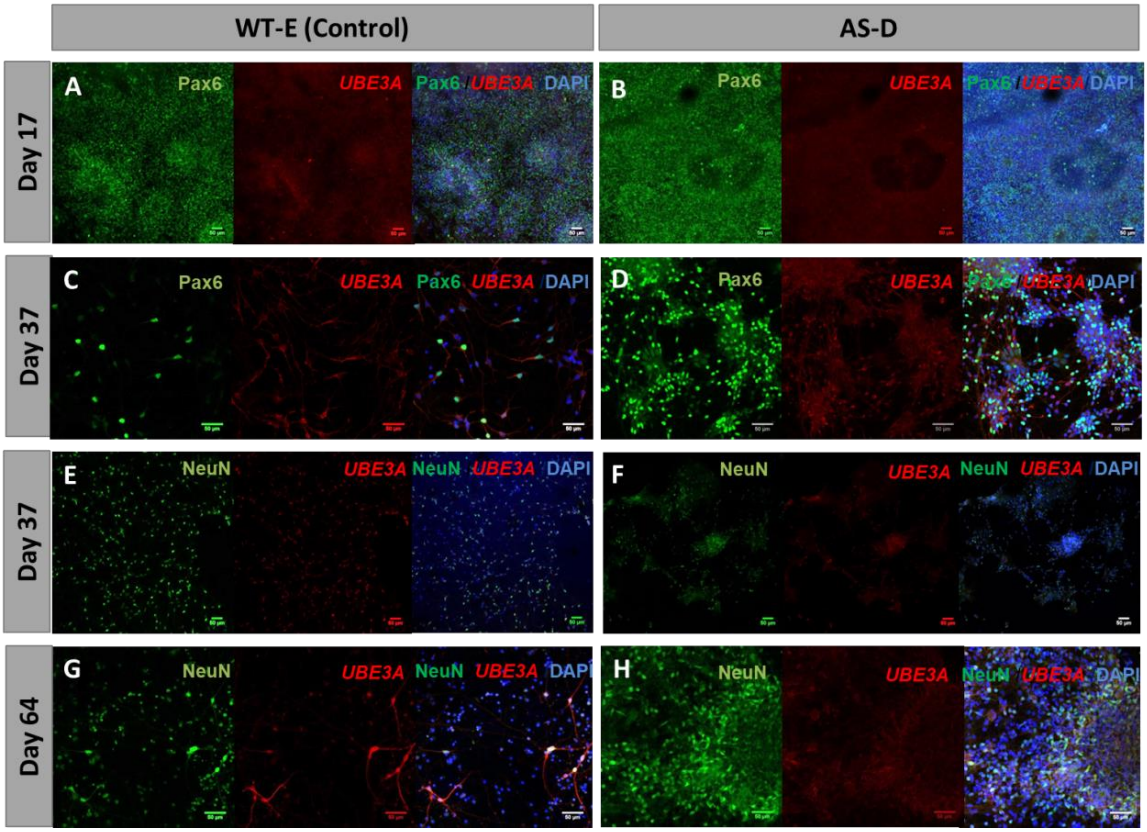

Figure IV. 10 : Confocal microscopy images of immunofluorescence staining for control (WT-E) and Angelman (AS-D) derived from human iPSCs at different stages of the neural commitment protocol using N2B27 medium and laminin-coated surfaces. A, B, C, D - At days 17 and 37 of differentiation, immunostaining analysis was performed for the typical neural progenitor marker Pax6 and for *UBE3A* either in control and Angelman-derived cells (scale bars: 50 µm). E, F, G, H - At days 37 and 63 cells were marked with mature neuron marker NeuN and *UBE3A* either in control and Angelman-derived cells (scale bars: 50 µm). Total cells were stained with DAPI and the images obtained with immuno- and DAPI staining were merged together (Scale bars – 50 µm).

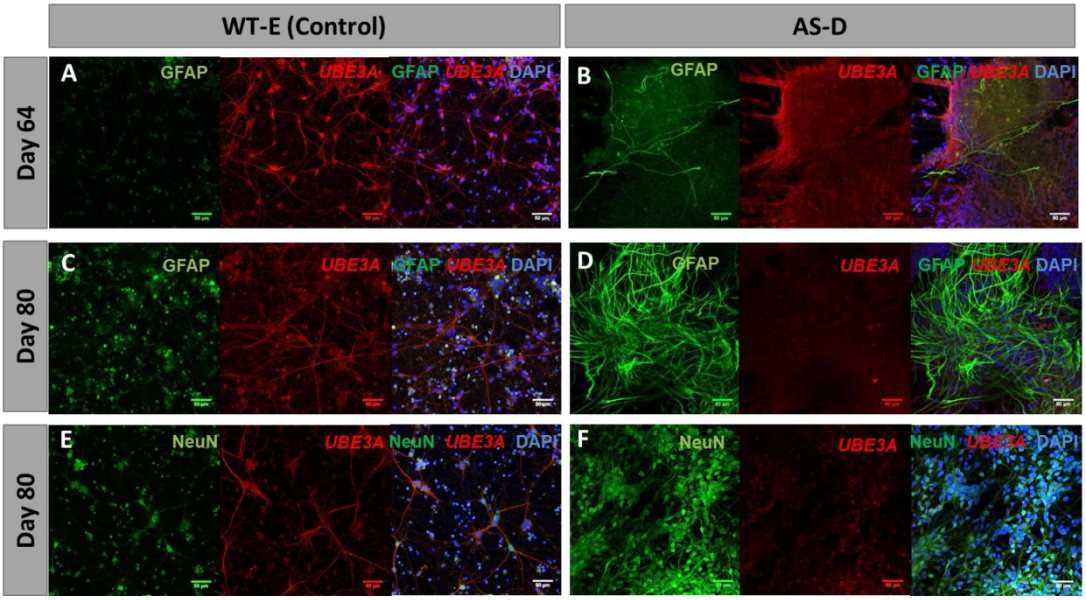

Figure IV. 11 : Confocal microscopy images of immunofluorescence staining for control (WT-E) and Angelman (AS-D) derived from human iPSCs at different stages of the neural commitment protocol using N2B27 medium and laminin-coated surfaces. A, B, C, D - At days 63 and 80 of differentiation, immunostaining analysis was performed for GFAP, an astrocyte marker and for *UBE3A* either in control and Angelman-derived cells (scale bars: 50 µm). E, F - At day 80, cells were marked with mature neuron marker NeuN and *UBE3A* either in control and Angelman-derived cells (scale bars: 50 µm). Total cells were stained with DAPI and the images obtained with immuno- and DAPI staining were merged together (Scale bars – 50 µm).

We then analyzed *UBE3A* expression during neuronal differentiation by IF. Expression was found to be low at day 17, a phase where most cells express high levels of *PAX6* (which interestingly was mostly found in AS-D rather than in WT- E) (figure IV.10A and IV.10B). Interestingly, some *UBE3A* positive neural progenitors could be seen in control, which corroborates the expression by RT-qPCR for *UBE3A* at this stage, in which it was starting to rise and was more evident in control than Angelman-derived neural progenitors (figure IV.9).

From day 37, *UBE3A* expression starts showing significant differences in the pattern of expression between the two cell lines (figure IV.10C and IV.10D). In WT-E, there were a higher number of positive neurons for *UBE3A* compared to the AS-D line in which the expression of *UBE3A* increased slightly at this stage (figure IV.10E and IV.10F).

At day 64, was possible to see a significant increase of *UBE3A* expression in control cells. UBE3A marked cells always co-localized NeuN expression, indicating these cells are neurons. A homogeneous positive neuronal population for *UBE3A* was seen for control neurons, information that is sustained by a majority of NeuN positive cells for *UBE3A* at this stage. In Angelman-derived neurons, *UBE3A* staining was much fainter than control neurons, although it is still present to some extent meaning that UBE3A repression might start to occur, but is not complete at this stage (figure IV.10G and IV.10H).

Next, the GFAP staining, which marks astrocytes, was evaluated to understand whether *UBE3A* co-stains or not with astrocytes. Regarding that, there is an evident difference in control and Angelman-derived cells since in control the majority of the population presents no GFAP-positive cells, while in

AS-D GFAP-positive astrocytes are visible particularly in certain regions of the culture. In addition, there is no co-localization between UBE3A and GFAP (figure IV.11A and IV.11B).

On day 80, we were able to see a significant increase in UBE3A expression in the control cell line compared to day 37, which is coherent with RT-qPCR results at this stage (figure IV.9). In the case of the AS-D cell line, the population of *UBE3A* negative neurons was even more noticeable since the majority of neurons present in AS-D at this stage are NeuN positive and *UBE3A* negative, meaning that imprinting that result in the inactivation of *UBE3A* might have occurred in most of the neurons. However, some UBE3A+ population was still present, which is coherent with the expression profiles obtained for this stage (figure IV.11E and IV.11F).

Also at day 80, a substantial number of widespread neuronal projections were observed only in AS-D cell line. Furthermore, GFAP-positive astrocytes could be seen (figure IV.11C and IV.11D). Interestingly, GFAP was present in a greater amount in AS and this was an intriguing result from this experiment since studies by Fink *et al* showed no significantly differences for AS and control cultures based on of S-100 Protein Subunit Beta (S100 β), a mature astrocyte marker [86]. Since our studies demonstrated that this behavior is noticed only in AS-D but not in control cell line, this might be a specific feature of Angelman syndrome. To confirm this hypothesis, more tests must be performed in the future.

Taken together, this result suggests that in terms of *UBE3A* expression, the majority of neurons present in AS-D at day 80 are NeuN positive and *UBE3A* negative and for WT-E there is an opposite behavior. This findings might indicate that *UBE3A* imprinting not occurred totally at this timepoint since there is still some *UBE3A* expression but a high amount of neurons seemed to already inactivate *UBE3A*, corroborating with the fact that the silencing of paternal *UBE3A* expression occurs only late during neuronal differentiation [85].

V. Conclusions and Future Remarks

The general aim of this dissertation was to develop a human model system for Angelman Syndrome based on the induction of neuronal differentiation *in vitro* using control and Angelman-derived iPSCs by a dual-SMAD inhibition protocol.

First, to demonstrate the pluripotency state of both iPSC control and Angelman-derived cell lines, a flow cytometry analysis was performed for the main pluripotency markers SSEA4, TRA-1-60, OCT4 and SOX2. This analysis indicated a pluripotent state of these cell populations before neural commitment protocol since all the pluripotency-associates markers tested showed a high percentage of positive staining (>80 %).

Then, the neuronal differentiation procedure was accomplished using the dual-SMAD inhibition protocol, combining both inhibiting small molecules, SB-431542 and LDN-193189 with N2B27 medium, after a 100 % confluence of iPSC population was attained, during 12 days of neural commitment protocol.

A neural commitment characterization of neural progenitor markers was performed by IF staining. These analyses revealed a majority of cells that were certainly positive for PAX6 and NESTIN, either in control and Angelman-derived cells. RT-qPCR expression profiles for these markers confirmed the authenticity of IF staining.
In general, no significant differences were observed, as both Angelman-derived and control cultures showed an expected immature neural phenotype. Nevertheless, Angelman-derived culture presented significantly more cell density along all the differentiation process with more proliferative capacity in comparison with control which starts being noticeable from day 12.

After 12 days of neural induction in dual-SMAD inhibition protocol, immature NPs were replated onto laminin-coated plates and supplement with bFGF growth factor during 3 days. At day 17, SOX2 staining revealed the presence of neural rosette structures that gave rise to TUJ1-positive immature new born neurons outgrowing from neural rosettes, around day 28 of neural commitment protocol.
As expected, after peaking during the initial stage of neural commitment, expression of typical neural markers (PAX6 and NESTIN) declined during further differentiation and a progressive appearance of the neuronal marker beta III-tubulin (TUJ1) became more evident. Taking together, the results obtained for these markers by IF and the expression profiles acquired by RT-qPCR have proven that the neural induction was in accordance with the published literature[39].

Afterwards, the neuronal differentiation protocol proceeded with the replacement of N2B27 by the Maturation N2B27, with formulation specifications previously described in section III.2.2.
IF staining analysis for mature neuronal markers at day 64 unveiled the predominance of GAD65 positive cell population in control in comparison with Angelman-derived neurons in which the expression is absent for this marker. The same features can be perceived for the VGAT staining at days 64 and 80. At day 64, a substantial fraction of neurons were positive for VGAT at day 64 in

control neurons, while a comparatively less and more heterogeneous staining for this marker was observed in Angelman-derived neurons (figure IV. 6D). In addition, at day 80, there was a significant increase in expression of this marker, which was only detectable for control neurons.
Taken together, these results confirmed a majority of GABAergic neurons for control in comparison with Angelman-derived neurons which were corroborated by RT-qPCR results.

Regarding VGLUT1 expression, the RT-qPCR analysis showed a strong upregulation of this marker, only for AS-D at later stages of neuronal maturation, a finding not observed for the WT-E control neurons. In the future, the use of a specific marker for glutamatergic neurons should be tested to validate the obtained RT-qPCR results.

Furthermore, concerning the morphological features observed either in control and Angelman-derived cell lines, a widespread neuronal population with small aggregates with a rounder shape arrangement was observed at day 64 for the control line. As for Angelman-derived iPSCs, it is clear the significant presence of interconnected, non-uniform aggregates. These phenotypic differences may be the result of potential physiological abnormalities driven by the disease.

To further demonstrate the robustness of this system as a model for Angelman syndrome, neuronal identity and imprinted expression of the Angelman locus in the generated cells were explored. Also, further analyses regarding the evaluation of the methylation status of PWS-IC region and expression profiles of *UBE3A* during neuronal differentiation were executed.

First, the methylation pattern of the PWS-IC region of chromosome 15q11-q13 was studied in the Control and Angelman-derived cells in several timepoints (days 0, 37 and 80) by COBRA. This analysis revealed that the imprinting status was maintained during the neuronal differentiation in both iPSC lines, which suggests that this could be a robust disease modelling platform to study Angelman syndrome.

The other crucial feature of a proper AS model is the gradual repression of the paternal *UBE3A* allele along the differentiation process. To check whether this repression occurred along the differentiation protocol and particularly to discover when and in which cells the paternal *UBE3A* imprinting occurs, we perform IF and RT-qPCR analysis from day 0 to day 80, to study *UBE3A* expression in both normal and AS cultures. For this purpose, we also tried nascent-transcript RNA FISH for *UBE3A* gene, but this experiment did not worked unfortunately. RT-qPCR analysis for *SNORD115* was also performed since this gene is supposed to be expressed only in neurons and to match the expression of the *UBE3A-ATS*, which is involved in the silencing of the paternal *UBE3A* gene.

During the neuronal differentiation protocol, *UBE3A* expression showed an evident increase that is highly noticed in later stages of neuronal development for control neurons. As for AS cell line we observed a gradual decay of *UBE3A* expression that was more pronounced at day 80 of neuronal differentiation. Nevertheless, some neurons remained positive for *UBE3A* at this stage, which is coherent with *UBE3A* RT-qPCR expression profiles that showed a basal expression of this gene. In

conclusion, *UBE3A* is not totally repressed and *UBE3A* imprinting might have started but was not completed by day 80 of this neuronal differentiation protocol. To validate this hypothesis, one approach would be the extension of this neuronal differentiation until later stages of maturation to discover if *UBE3A* decay was more evident. This approach might be promising since this protocol can be further extended, similar to what was done in the past by Fernandes *et al* [39], ensuring even more maturation of the neurons. Moreover, we should also re-try nascent transcript RNA FISH, an experiment that will be the ultimate test to reveal whether *UBE3A* imprinting had or not occurred.

Concerning *SNORD115* expression, the expression profiles obtained in later stages of neuronal differentiation were not in accordance with previous studies that showed an up-regulation of this gene upon 70 days of differentiation [85]. Unexpectedly, the expression of *SNORD115* was found markedly reduced in AS-D from day 37 of differentiation when compared to control. The reasons behind such a difference are difficult to explain. One hypothesis behind such a difference might be that *SNORD115* levels of expression are higher in GABAergic neurons which are strongly reduced in AS-D neurons in comparison with glutamatergic neurons. Nevertheless, in the future, these analyses must be repeated to acquire a more conclusive result, and the expression profiles of *UBE3A-ATS* must also be tested using a specific primer for this long non-coding RNA transcribed in the antisense orientation and overlapping with the *UBE3A* gene.

Another aspect that can be dissected to demonstrate the differences between AS and Control differentiation protocols would be the presence of glia cells, namely astrocytes, that were also detected by staining with glial fibrillary acidic protein (GFAP).
Angelman-derived cells revealed a considerable population that presented GFAP-positive staining, which was particularly high at later stages of the neuronal differentiation protocol. As for the control, the majority of cells presented GFAP- negative staining. In addition, there is no co-localized staining for *UBE3A* either in control or Angelman-derived cultures.
Since this behavior is noticed only in AS-D but not in control cell line, this might be a specific feature of Angelman syndrome. To confirm this hypothesis, it could be advantageous the implementation of this protocol using other Angelman-derived iPSCs cell lines, and compare again with the control to attest the authenticity of these previously obtained results to better understand whether these phenotypes are replicated.

Taken together, these results suggest that in terms of *UBE3A* expression, the majority of neurons present in AS-D at day 80 are NeuN positive and *UBE3A* negative and for WT-E there is an opposite behavior. These findings might indicate that *UBE3A* imprinting not occurred totally at this timepoint since there is still some *UBE3A* expression but a high amount of $NeuN^+$ cells have already inactivate *UBE3A*. Nevertheless, a considerable variability in differentiation efficiency must be considered, since several studies deal with this same problematic along iPSCs differentiation [85,94].
Regarding that, further studies will be necessary to validate this hypothesis, applying these same techniques and methodology to other Angelman-derived hiPSCs cell lines, to attest if the same behavior is observed independently of the cell line.

Future work must also be focused on the functionality of the generated neurons, since maturity of neural population seems to be heterogeneous given the specific arrangement and heterogeneity displayed in Angelman- derived neurons during the neuronal differentiation protocol. For that, electrophysiology analysis must be performed to attest the synaptic activity pattern in both cultures, particularly in the AS culture system.

Thus, this successfully human cell culture model for AS could be used also to better understand the mechanisms of the disease and develop distinctive tools for drug discovery. More specifically, we can assess the treatment of AS-neurons with modified antisense oligonucleotide (ASOs) against *UBE3A-ATS* transcript and test for *UBE3A* activation and phenotypic improvement. Such a strategy might be useful to find suitable conditions to activate the normally silent paternal allele of the U*BE3A* gene in order to advance towards a future treatment for AS patients.

VI. References

1. Meng, L. *et al.* Towards a therapy for Angelman syndrome by targeting a long non-coding RNA. *Nature* (2015). doi:10.1038/nature13975

2. Tan, W.-H. & Bird, L. M. Pharmacological therapies for Angelman syndrome. *Wiener Medizinische Wochenschrift* (2016). doi:10.1007/s10354-015-0408-z

3. Williams, C. a, Driscoll, D. J. & Dagli, A. I. Clinical and genetic aspects of Angelman syndrome. *Genet. Med.* (2010). doi:10.1097/GIM.0b013e3181def138

4. Margolis, S. S., Sell, G. L., Zbinden, M. A. & Bird, L. M. Angelman Syndrome. *Neurotherapeutics* (2015). doi:10.1007/s13311-015-0361-y

5. Lossie, a C. *et al.* Distinct phenotypes distinguish the molecular classes of Angelman syndrome. *J. Med. Genet.* (2001). doi:10.1136/jmg.38.12.834

6. Hoffmann, K. & Heller, R. Uniparental disomies 7 and 14. *Best Pract. Res. Clin. Endocrinol. Metab.* (2011). doi:10.1016/j.beem.2010.09.004

7. Sell, G. L. & Margolis, S. S. From UBE3A to Angelman syndrome: A substrate perspective. *Frontiers in Neuroscience* (2015). doi:10.3389/fnins.2015.00322

8. Thibert, R. L., Larson, A. M., Hsieh, D. T., Raby, A. R. & Thiele, E. A. Neurologic manifestations of Angelman syndrome. *Pediatric Neurology* (2013). doi:10.1016/j.pediatrneurol.2012.09.015

9. Gentile, J. K. *et al.* A neurodevelopmental survey of Angelman syndrome with genotype-phenotype correlations. *J. Dev. Behav. Pediatr.* (2010). doi:10.1097/DBP.0b013e3181ee408e

10. Bird, L. M. Angelman syndrome: Review of clinical and molecular aspects. *Application of Clinical Genetics* (2014). doi:10.2147/TACG.S57386

11. Soucy, E. A. *et al.* A Pilot Study for Evaluation of Hypotonia in Children With Neurofibromatosis Type 1. *J. Child Neurol.* **30,** 382–385 (2015).

12. LaSalle, J. M., Reiter, L. T. & Chamberlain, S. J. Epigenetic regulation of UBE3A and roles in human neurodevelopmental disorders. *Epigenomics* (2015). doi:10.2217/epi.15.70

13. Dindot, S. V., Antalffy, B. A., Bhattacharjee, M. B. & Beaudet, A. L. The Angelman syndrome ubiquitin ligase localizes to the synapse and nucleus, and maternal deficiency results in abnormal dendritic spine morphology. *Hum. Mol. Genet.* (2008). doi:10.1093/hmg/ddm288

14. Chamberlain, S. J. RNAs of the human chromosome 15q11-q13 imprinted region. *Wiley Interdisciplinary Reviews: RNA* (2013). doi:10.1002/wrna.1150

15. Gray, T. A., Saitoh, S. & Nicholls, R. D. An imprinted, mammalian bicistronic transcript encodes two independent proteins. *Proc. Natl. Acad. Sci.* (1999). doi:10.1073/pnas.96.10.5616

16. Pólvora-brandão, A. D., Joaquim, M. & Godinho, I. Loss of hierarchical imprinting regulation at the Prader-Willi/Angelman syndrome locus in human iPSCs. 1–41 (2018). doi:10.1093/hmg/ddy274/5068136

17. Meng, L., Person, R. E. & Beaudet, A. L. Ube3a-ATS is an atypical RNA polymerase II transcript that represses the paternal expression of Ube3a. *Hum. Mol. Genet.* (2012). doi:10.1093/hmg/dds130

18. Stanurova, J. *et al.* Angelman syndrome-derived neurons display late onset of paternal UBE3A silencing. *Sci. Rep.* (2016). doi:10.1038/srep30792

19. Ramsden, S. C., Clayton-Smith, J., Birch, R. & Buiting, K. Practice guidelines for the molecular analysis of Prader-Willi and Angelman syndromes. *BMC Med. Genet.* (2010). doi:10.1186/1471-2350-11-70

20. Wheeler, A. C., Sacco, P. & Cabo, R. Unmet clinical needs and burden in Angelman syndrome: A review of the literature. *Orphanet Journal of Rare Diseases* (2017). doi:10.1186/s13023-017-0716-z

21. Bi, X., Sun, J., Ji, A. X. & Baudry, M. Potential therapeutic approaches for Angelman syndrome. *Expert Opin Ther Targets* (2016). doi:10.1517/14728222.2016.1115837

22. Huang, H. S. *et al.* Topoisomerase inhibitors unsilence the dormant allele of Ube3a in neurons. *Nature* (2012). doi:10.1038/nature10726

23. Daily, J. L. *et al.* Adeno-associated virus-mediated rescue of the cognitive defects in a mouse model for Angelman syndrome. *PLoS One* (2011). doi:10.1371/journal.pone.0027221

24. Powell, W. T. *et al.* R-loop formation at *Snord116* mediates topotecan inhibition of *Ube3a-antisense* and allele-specific chromatin decondensation. *Proc. Natl. Acad. Sci.* (2013). doi:10.1073/pnas.1305426110

25. Rinaldi, C. & Wood, M. J. A. Antisense oligonucleotides: the next frontier for treatment of neurological disorders. *Nat. Rev. Neurol.* (2017). doi:10.1038/nrneurol.2017.148

26. Kirschstein, R. (National I. of H. & Skirboll, L. R. (National I. of H. *Stem cells: Scientific progress and future research directions*. *NIH - Department of Health and Human Services* (2001).

27. Hui, H. *et al.* Stem Cells : General Features and Characteristics. *Stem Cells Clin. Res.* 1–20 (2011). doi:10.5772/740

28. Lodi, D., Iannitti, T. & Palmieri, B. Stem cells in clinical practice: applications and warnings. *J.*

Exp. Clin. Cancer Res. (2011). doi:10.1186/1756-9966-30-9

29. TIBI PUIU. Massive database of of 1,500 stem cell lines derived from diseased cells set to aid drug development. Available at: https://www.zmescience.com/research/stembancc-project-1500-stem-cell-lines/. (Accessed: 19th August 2018)

30. Article, R. *et al.* A Review : Stem Cells and Classification of Stem Cells. **5,** 534–556 (2016).

31. Daley, G. Q. Stem cells and the evolving notion of cellular identity. *Philosophical Transactions of the Royal Society B: Biological Sciences* (2015). doi:10.1098/rstb.2014.0376

32. Singh, V. K., Saini, A., Kalsan, M., Kumar, N. & Chandra, R. Describing the Stem Cell Potency: The Various Methods of Functional Assessment and In silico Diagnostics. *Front. Cell Dev. Biol.* (2016). doi:10.3389/fcell.2016.00134

33. Takahashi, K. & Yamanaka, S. Induction of Pluripotent Stem Cells from Mouse Embryonic and Adult Fibroblast Cultures by Defined Factors. *Cell* (2006). doi:10.1016/j.cell.2006.07.024

34. Wiederschain, G. Y. Essentials of glycobiology. *Biochem.* (2009). doi:10.1134/S0006297909090156

35. De Los Angeles, A. *et al.* Hallmarks of pluripotency. *Nature* (2015). doi:10.1038/nature15515

36. Jaenisch, R. & Young, R. Stem Cells, the Molecular Circuitry of Pluripotency and Nuclear Reprogramming. *Cell* (2008). doi:10.1016/j.cell.2008.01.015

37. Mitalipov, S. & Wolf, D. Totipotency, pluripotency and nuclear reprogramming. *Adv. Biochem. Eng. Biotechnol.* (2009). doi:10.1007/10_2008_45

38. Loperfido, M., Steele-Stallard, H. B., Tedesco, F. S. & VandenDriessche, T. Pluripotent stem cells for gene therapy of degenerative muscle diseases. *Curr. Gene Ther.* (2015). doi:10.2174/1566523215666150630121207

39. Fernandes, T. G. *et al.* Neural commitment of human pluripotent stem cells under defined conditions recapitulates neural development and generates patient-specific neural cells. *Biotechnol. J.* (2015). doi:10.1002/biot.201400751

40. Thomson, J. A. *et al.* Embryonic stem cell lines derived from human blastocysts. *Science* (1998). doi:10.1126/science.282.5391.1145

41. Takahashi, K., Okita, K., Nakagawa, M. & Yamanaka, S. Induction of pluripotent stem cells from fibroblast cultures. *Nat. Protoc.* (2007). doi:10.1038/nprot.2007.418

42. Takahashi, K. *et al.* Induction of Pluripotent Stem Cells from Adult Human Fibroblasts by Defined Factors. *Cell* (2007). doi:10.1016/j.cell.2007.11.019

43. Fernandes, T. G., Rodrigues, C. A. V., Diogo, M. M. & Cabral, J. M. S. Stem cell bioprocessing

for regenerative medicine. *Journal of Chemical Technology and Biotechnology* (2014). doi:10.1002/jctb.4189

44. Yu, J. *et al.* Induced pluripotent stem cell lines derived from human somatic cells. *Science* (2007). doi:10.1126/science.1151526

45. Martin, P. E., Shaughnessy, E. M. O., Wright, C. S. & Graham, A. The potential of human induced pluripotent stem cells for modelling diabetic wound healing in vitro. 1629–1643 (2018).

46. Yamanaka, S. A Fresh Look at iPS Cells. *Cell* (2009). doi:10.1016/j.cell.2009.03.034

47. Chang, C.-Y. *et al.* Induced Pluripotent Stem Cells. *Cell Transplant.* 096368971877540 (2018). doi:10.1177/0963689718775406

48. Koch, P., Kokaia, Z., Lindvall, O. & Brüstle, O. Emerging concepts in neural stem cell research: autologous repair and cell-based disease modelling. *The Lancet Neurology* (2009). doi:10.1016/S1474-4422(09)70202-9

49. Ährlund-Richter, L. *et al.* Isolation and Production of Cells Suitable for Human Therapy: Challenges Ahead. *Cell Stem Cell* (2009). doi:10.1016/j.stem.2008.11.012

50. Lindvall, O., Kokaia, Z. & Martinez-Serrano, A. Stem cell therapy for human neurodegenerative disorders-how to make it work. *Nat. Med.* (2004). doi:10.1038/nm1064

51. Lindvall, O. & Kokaia, Z. Prospects of stem cell therapy for replacing dopamine neurons in Parkinson's disease. *Trends in Pharmacological Sciences* (2009). doi:10.1016/j.tips.2009.03.001

52. Lu, J., Delli-Bovi, L. C., Hecht, J., Folkerth, R. & Sheen, V. L. Generation of neural stem cells from discarded human fetal cortical tissue. *J. Vis. Exp.* (2011). doi:10.3791/2681

53. Mayer, E. J. *et al.* Neural progenitor cells from postmortem adult human retina. *Br. J. Ophthalmol.* (2005). doi:10.1136/bjo.2004.057687

54. Conti, L. & Cattaneo, E. Neural stem cell systems: Physiological players or in vitro entities? *Nature Reviews Neuroscience* (2010). doi:10.1038/nrn2761

55. Chojnacki, A. K., Mak, G. K. & Weiss, S. Identity crisis for adult periventricular neural stem cells: Subventricular zone astrocytes, ependymal cells or both? *Nature Reviews Neuroscience* (2009). doi:10.1038/nrn2571

56. Temple, S. The development of neural stem cells. *Nature* (2001). doi:10.1038/35102174

57. Götz, M. & Huttner, W. B. The cell biology of neurogenesis. *Nature Reviews Molecular Cell Biology* (2005). doi:10.1038/nrm1739

58. Elkabetz, Y. *et al.* Human ES cell-derived neural rosettes reveal a functionally distinct early

neural stem cell stage. *Genes Dev.* (2008). doi:10.1101/gad.1616208

59. Puelles, E. Otx2 Controls Identity and Fate of Glutamatergic Progenitors of the Thalamus by Repressing GABAergic Differentiation. *J. Neurosci.* (2006). doi:10.1523/JNEUROSCI.1097-06.2006

60. Banasr, M. *et al.* Characterization of GABAergic marker expression in the chronic unpredictable stress model of depression. *Chronic Stress (Thousand Oaks, Calif.)* **1,** (2017).

61. Tremblay, R., Lee, S. & Rudy, B. GABAergic Interneurons in the Neocortex: From Cellular Properties to Circuits. *Neuron* (2016). doi:10.1016/j.neuron.2016.06.033

62. Varoqui, H., Schäfer, M. K. H., Zhu, H., Weihe, E. & Erickson, J. D. Identification of the differentiation-associated Na+/PI transporter as a novel vesicular glutamate transporter expressed in a distinct set of glutamatergic synapses. *J. Neurosci.* **22,** 142–55 (2002).

63. Fremeau, R. T., Voglmaier, S., Seal, R. P. & Edwards, R. H. VGLUTs define subsets of excitatory neurons and suggest novel roles for glutamate. *Trends in Neurosciences* (2004). doi:10.1016/j.tins.2003.11.005

64. Park, S. K. *et al.* Vesicular glutamate transporter 1 (VGLUT1)- and VGLUT2-immunopositive axon terminals on the rat jaw-closing and jaw-opening motoneurons. *Brain Struct. Funct.* **223,** 2323–2334 (2018).

65. Zheng, W. *et al.* Differentiation of Glial Cells From hiPSCs: Potential Applications in Neurological Diseases and Cell Replacement Therapy. *Front. Cell. Neurosci.* **12,** 239 (2018).

66. Zhang, S. C. Defining glial cells during CNS development. *Nat. Rev. Neurosci.* (2001). doi:10.1038/35097593

67. Barres, B. A. The Mystery and Magic of Glia: A Perspective on Their Roles in Health and Disease. *Neuron* (2008). doi:10.1016/j.neuron.2008.10.013

68. Jäkel, S. & Dimou, L. Glial Cells and Their Function in the Adult Brain: A Journey through the History of Their Ablation. *Front. Cell. Neurosci.* (2017). doi:10.3389/fncel.2017.00024

69. Mertens, J., Marchetto, M. C., Bardy, C. & Gage, F. H. Evaluating cell reprogramming, differentiation and conversion technologies in neuroscience. *Nature Reviews Neuroscience* (2016). doi:10.1038/nrn.2016.46

70. Zhang, S. C., Wernig, M., Duncan, I. D., Brüstle, O. & Thomson, J. A. In vitro differentiation of transplantable neural precursors from human embryonic stem cells. *Nat. Biotechnol.* (2001). doi:10.1038/nbt1201-1129

71. Ziv, O. *et al.* Quantitative Live Imaging of Human Embryonic Stem Cell Derived Neural Rosettes Reveals Structure-Function Dynamics Coupled to Cortical Development. *PLoS*

Comput. Biol. (2015). doi:10.1371/journal.pcbi.1004453

72. Muratore, C. R., Srikanth, P., Callahan, D. G. & Young-Pearse, T. L. Comparison and optimization of hiPSC forebrain cortical differentiation protocols. *PLoS One* (2014). doi:10.1371/journal.pone.0105807

73. Pera, M. F. & Tam, P. P. L. Extrinsic regulation of pluripotent stem cells. *Nature* (2010). doi:10.1038/nature09228

74. Murry, C. E. & Keller, G. Differentiation of Embryonic Stem Cells to Clinically Relevant Populations: Lessons from Embryonic Development. *Cell* (2008). doi:10.1016/j.cell.2008.02.008

75. Chambers, S. M. *et al.* Highly efficient neural conversion of human ES and iPS cells by dual inhibition of SMAD signaling. *Nat. Biotechnol.* (2009). doi:10.1038/nbt.1529

76. Smith, J. R. *et al.* Inhibition of Activin/Nodal signaling promotes specification of human embryonic stem cells into neuroectoderm. *Dev. Biol.* **313,** 107–117 (2008).

77. Inman, G. J. SB-431542 Is a Potent and Specific Inhibitor of Transforming Growth Factor-beta Superfamily Type I Activin Receptor-Like Kinase (ALK) Receptors ALK4, ALK5, and ALK7. *Mol. Pharmacol.* (2002). doi:10.1124/mol.62.1.65

78. Greber, B., Lehrach, H. & Adjaye, J. Fibroblast growth factor 2 modulates transforming growth factor beta signaling in mouse embryonic fibroblasts and human ESCs (hESCs) to support hESC self-renewal. *Stem Cells* (2007). doi:10.1634/stemcells.2006-0476

79. James, D. TGF /activin/nodal signaling is necessary for the maintenance of pluripotency in human embryonic stem cells. *Development* (2005). doi:10.1242/dev.01706

80. Boergermann, J. H., Kopf, J., Yu, P. B. & Knaus, P. Dorsomorphin and LDN-193189 inhibit BMP-mediated Smad, p38 and Akt signalling in C2C12 cells. *Int. J. Biochem. Cell Biol.* (2010). doi:10.1016/j.biocel.2010.07.018

81. Egashira, T., Yuasa, S. & Fukuda, K. Stem Cell Research for Regenerative Medicine / Personalized Medicine Novel Insights into Disease Modeling Using Induced Pluripotent Stem Cells. *Biol. Pharm. Bull.* **36,** 182–188 (2013).

82. Onder, T. T. & Daley, G. Q. New lessons learned from disease modeling with induced pluripotent stem cells. *Current Opinion in Genetics and Development* (2012). doi:10.1016/j.gde.2012.05.005

83. Van den Ameele, J., Tiberi, L., Vanderhaeghen, P. & Espuny-Camacho, I. Thinking out of the dish: What to learn about cortical development using pluripotent stem cells. *Trends in Neurosciences* (2014). doi:10.1016/j.tins.2014.03.005

84. Amir, R. E. & Zoghbi, H. Y. Rett syndrome: Methyl-CpG-binding protein 2 mutations and phenotype-genotype correlations. *Am. J. Med. Genet. - Semin. Med. Genet.* (2000). doi:10.1002/1096-8628(200022)97:2<147::AID-AJMG6>3.0.CO;2-O

85. Chamberlain, S. J. *et al.* Induced pluripotent stem cell models of the genomic imprinting disorders Angelman and Prader–Willi syndromes. *Proc. Natl. Acad. Sci.* (2010). doi:10.1073/pnas.1004487107

86. Fink, J. J. *et al.* Disrupted neuronal maturation in Angelman syndrome-derived induced pluripotent stem cells. *Nat. Commun.* (2017). doi:10.1038/ncomms15038

87. Avior, Y., Sagi, I. & Benvenisty, N. Pluripotent stem cells in disease modelling and drug discovery. *Nature Reviews Molecular Cell Biology* (2016). doi:10.1038/nrm.2015.27

88. Beers, J. *et al.* Passaging and colony expansion of human pluripotent stem cells by enzyme-free dissociation in chemically defined culture conditions. *Nat. Protoc.* (2012). doi:10.1038/nprot.2012.130

89. Shi, Y., Kirwan, P. & Livesey, F. J. Directed differentiation of human pluripotent stem cells to cerebral cortex neurons and neural networks. *Nat. Protoc.* (2012). doi:10.1038/nprot.2012.116

90. Lendahl, U., Zimmerman, L. B. & McKay, R. D. CNS stem cells express a new class of intermediate filament protein. *Cell* (1990). doi:10.1016/0092-8674(90)90662-X

91. Liu, H., Li, F., Wang, C. & Su, Z. More sensitivity of cortical GABAergic neurons than glutamatergic neurons in response to acidosis. *Neuroreport* **27,** 610–616 (2016).

92. Chamberlain, S. J. & Lalande, M. Angelman Syndrome, a Genomic Imprinting Disorder of the Brain. *J. Neurosci.* (2010). doi:10.1523/JNEUROSCI.1728-10.2010

93. Gusel'nikova, V. V. & Korzhevskiy, D. E. NeuN as a neuronal nuclear antigen and neuron differentiation marker. *Acta Naturae* (2015).

94. Hu, B.-Y. *et al.* Neural differentiation of human induced pluripotent stem cells follows developmental principles but with variable potency. *Proc. Natl. Acad. Sci.* (2010). doi:10.1073/pnas.0910012107